Industrial Crops & Products 160 (2021) 113123

Contents lists available at ScienceDirect

Industrial Crops & Products

journal homepage: www.elsevier.com/locate/indcrop

Effect of main solid biomass commodities of patula pine on biochar properties produced under gasification conditions

Jonatan Gutiérrez [a,b], Ainhoa Rubio-Clemente [b,c], Juan F. Pérez [a,*]

[a] Grupo de Manejo Eficiente de la Energía – Gimel, Departamento de Ingeniería Mecánica, Facultad de Ingeniería, Universidad de Antioquia, Calle 67, No. 53-108, Medellín, Colombia
[b] Grupo Energía Alternativa, Departamento de Ingeniería Mecánica, Facultad de Ingeniería, Universidad de Antioquia, Calle 67, No. 53-108, Medellín, Colombia
[c] Facultad de Ingeniería, Tecnológico de Antioquia–Institución Universitaria TdeA, Calle 78b, No. 72A-220, Medellín, Colombia

ARTICLE INFO

Keywords:
Wood chips and pellets
Fixed-bed reactor
Gasification biochar
Solid biofuel
Byproduct recovery
Pyrolysis kinetics

ABSTRACT

Wood pellets (WP) and chips (WCH) are the most frequently sold products worldwide to produce bioenergy under thermochemical processes. The effects of the bulk density of patula pine (*Pinus patula*) WP (555.97 kg/m^3) and WCH (151.29 kg/m^3), and their gasification conditions were studied on the properties of the produced biochars (BCs). The aim of this study was to generate a good-quality gas fuel (producer gas), as well as a BC with properties that would enable it to be used as a solid biofuel instead of being considered as a byproduct or waste. An atmospheric reverse-downdraft gasifier was used, setting the air flow at 0.12 kg/m^2/s for the samples of biomasses studied. With regard to the gasification performance, the temperature inside the reactor was found to increase by 70 % for WP, obtaining a higher cold gas efficiency (51.6 %) in comparison with the efficiency achieved for WCH (36.7 %). Concerning the properties of the BCs, the highest gasification temperature allowed to reach a pellet-derived biochar (WP-BC) with a surface area (BET) larger than that one obtained for the chip-derived biochar (WCH-BC), with 367.33 m^2/g and 233.56 m^2/g, respectively. Furthermore, the WP-BC heating value was found to be 29.25 MJ/kg, while this parameter for the WCH-BC was 28.36 MJ/kg. It is highlighted the low probability of corrosion and ash fusion occurrence within the reactor when using these biofuels (raw and BCs). Additionally, regarding the pyrolysis kinetics of the raw biomasses, WCH showed a higher reactivity with an activation energy (E_α) of 80.84 kJ/mol in comparison with the E_α value obtained for WP (124.38 kJ/mol).

1. Introduction

In 2018, according to the United Nations Organization for Food and Agriculture (FAO), Colombia generated 623,000 m^3 of wood residue, 158,000 m^3 of chips and wood particles were produced, and a total of ~7.1 × 10^6 m^3 of fuel-intended wood was accounted for (FAO, 2019). As stated by the Agriculture and Rural Development Ministry (*Minagricultura*), the forest sector represents 0.2 % of the country gross domestic product (GDP) and has a forest potential of ~24 million ha for commercial exploitation (Minagricultura, 2015), which does not compete with agriculture nor the cattle industry, and are not inside the area reserved for jungle and tropical forests (Pérez and Ramírez, 2019). Colombia has forest species with a great dendroenergy potential, as it is the case of patula pine (*Pinus patula*). The annual yield of ~20 m^3/ha-year, the harvest time of ~13 years, and the planted area in the country of ~38,500 ha are regarded as some of the patula pine silvicultural properties standing out (Pérez et al., 2019). Therefore, patula pine can be defined as a reference to be used as a feedstock for energy production through thermo-chemical processes such as pyrolysis, hydrothermal, combustion, and gasification (Ramos-Carmona et al., 2018), among them the latter one is regarded as the best thermochemical process converting the biomass chemical energy into electrical energy (Montiel-Bohórquez and Pérez, 2019; Saghir et al., 2018). In addition to the benefits ascribed to the use of the gasification technique (an efficient electrical energy generation), it has environmental advantages, since gasification is adapted to the regulations worldwide applied in terms of polluting emissions (Arena, 2012). In fact, low temperatures in the gasification reactor reduce the particulate matter (PM_{10} and $PM_{2.5}$), sulphur oxides (SO_x) and nitrogen oxides (NO_x), in comparison with other biomass combustion processes (Ren et al., 2019; Sikarwar et al., 2016). Furthermore, gasification minimizes the fusion tendency of ashes within the reactor (Castaldi et al., 2017).

* Corresponding author.
E-mail address: juanpb@udea.edu.co (J.F. Pérez).

https://doi.org/10.1016/j.indcrop.2020.113123
Received 5 August 2020; Received in revised form 23 October 2020; Accepted 10 November 2020
Available online 26 November 2020

Gasification is a process in which biomass is degraded through chemical and thermal reactions in the presence of a limited amount of the oxidizing agent and at medium-high temperatures (higher than 700 °C). The main objective of the process is to produce a fuel gas, which is mainly composed of carbon monoxide (CO), carbon dioxide (CO_2), methane (CH_4), hydrogen (H_2), nitrogen (N_2), water vapor, and small amounts of heavy hydrocarbons (tars) (Perez et al., 2015). Biochar (BC) is obtained as a gasification byproduct (Hernández et al., 2016); a carbon-like solid residue resulting from the drying and thermal degradation of biomass constituents such as hemicellulose and cellulose. BC mass yield under biomass gasification regimes is ~10 % (Qian et al., 2014).

Currently, BC is considered a derivative with an added value since it is regarded as a cheap and an environmentally sustainable material, which can be used in several environmental and technological applications ("International Biochar Initiative," 2019), including the treatment of both organic and inorganic pollutants in water and soil (De Gisi et al., 2016; Díez and Pérez, 2019), the collection and storing of greenhouse gases (GHG) (Lin et al., 2015), the energy storage as supercapacitors (Gupta et al., 2015), and as catalysts in the tar treatment present in syngas (Gómez-Barea et al., 2013). Additionally, BC can be used in the biodiesel production (Bazargan et al., 2015), as well as a solid fuel directly applied in the gasification/combustion processes (Lee et al., 2020). This type of reutilization strategies are crucial for the contribution to the biomass sustainability as a renewable fuel (Iiyama et al., 2017).

The BC produced from the biomass gasification is a heterogeneous material, whose properties are influenced by the gasification technology, the operation conditions, and the raw material (Qian et al., 2013). Unlike the information reported on the pyrolytic BC, already used as a precursor of the activated carbon (Brudey et al., 2016), data on BC obtained from gasification plants are scarce (Hansen et al., 2015; Hernández et al., 2016). Some studies have reported the physicochemical characteristics of the gasification BC, which are essential for understanding the relation between the production conditions and the BC acquired properties and, subsequently, the identification of the best application for this derivative (Qian et al., 2015).

BC has been established to be used as a solid fuel due to its suitable heating value, 26–31 MJ/kg (Iiyama et al., 2017). This value can be comparable with coal, whose magnitude ranges between 28 and 32 MJ/kg (Harvey, 2010). In turn, the BC fixed carbon content has been reported to be ~70 % higher with respect to the fixed carbon content in the raw biomass (Misginna and Rajabu, 2014). In addition, it is worth noting that the BC gasification, in contrast with the biomass gasification, has some advantages ascribed, such as a less tar concentration in the syngas (Antal and Grønli, 2003) and a higher reactivity due to the BC porous structure (Duman et al., 2014). Nevertheless, the BC fuel value index (energy density) derived from the gasification is reduced (between ~55 % and ~85 %) when compared to the raw biomasses. Such as reduction can be attributed to the low bulk density of BCs due to the hemicellulose and cellulose degradation during the gasification process, and because of the ash content (AC) increase (Daniel et al., 2014; Díez and Pérez, 2019). Díez and Pérez (2019) found that the properties of the BC produced through the gasification of chips from different types of wood in a *top-lift updraft* (TLUD) reactor were affected by the biomass characteristics and the gasification temperature. The biomasses with a higher fuel value index (FVI) produced BCs with better properties as solid fuel, and the lower gasification temperatures allowed to obtain BCs with a higher heating value (27.71 MJ/kg) due to their reduced AC.

One alternative use of BC as a coproduct instead of as a byproduct of the gasification might be as a fuel through its recirculation inside the reactor. This would allow to have systems with a total energy efficiency higher than 90 % (Laird et al., 2009). Additionally, the biomass co-combustion with BC has been identified as one solution to reduce CO_2 emissions (Gao and Wu, 2011). In this regard, BCs can be also considered as sustainable biofuels (Clare et al., 2015) with the ability to reduce the pollution derived from thermochemical processes, due to their low sulfur and heavy metal contents (Balat, 2007).

In this work, BCs derived from patula pine wood chips (WCH) and wood pellets (WP) gasification process are characterized as solid biofuels. This fast-growing wood species has been selected because WCH and WP could be produced from harvest waste such as stems, sawdust, pruning remains, and sawmill waste, whose waste and pretreatment costs per ton are 0.0 and ~30−40 US$, respectively (Osorio et al., 2014). The objective of this work is to evaluate the effect of the raw material on the properties of the BC derived from the gasification of two types of the most common biomasses in the international market (chips and pellets) (Pérez and Ramírez, 2019). For this purpose, the effect of the gasification conditions on the BCs derived from chips (WCH-BC) and pellets (WP-BC) by using a reverse-downdraft reactor is assessed through the analysis of the physicochemical and energy properties. Furthermore, a reactivity analysis of the biomasses and their BCs is carried out under devolatilization conditions. With this research, the knowledge on the selection of the fuel type (chips or pellets) for the gasification to obtain a solid coproduct with added value and suitable properties to be used as a fuel in further thermochemical processes is intended to be broadened. It is important to note that BC could be potentially used as a soil amendment; therefore, the characterization of WCH-BC and WP-BC as amendment materials will be analyzed in further studies.

2. Materials and methods

2.1. Forest biomass used as a feedstock

The forestry sector is promoted by different incentives, such as the exemption from income tax on the exploitation of new forest crops; the Forestry Incentive Certificate; and funding of research programs and technological packages for the cultivation of pines and eucalyptus, among others species. These incentives seek to make feasible the forestry sector in Colombia (Pérez and Ramírez, 2019).

The wood biomass used was from patula pine (*Pinus patula*) due to its dendroenergy potential in Colombia (Pérez et al., 2019), as stated above. The forest biomass was gasified under the two most common worldwide forms for energy generation, WCH and WP (Hubbard, 2015; Whittaker and Shield, 2016). WCH were obtained from the *Bandit 95XP* equipment with particle sizes between 4 and 20 mm. In turn, WP were acquired commercially in a sawmill located in Medellin (Colombia), with a diameter and a length of 8 mm and from 10 to15 mm, respectively. It is highlighted that this particle size has been reported to be suitable for a stable oxidation under gasification processes (Lenis and Pérez, 2014; Pérez et al., 2012). The physicochemical properties of the two biomass types are presented in section 3.2.

2.2. Experimental installation

The gasification process was carried out in a reverse downdraft reactor (Fig. 1), which worked at an atmospheric pressure. The experimental installation was fitted with a supply line of air to be used as a gasifying agent. The air was supplied by a reciprocating compressor (2.6 kW, 3000 rpm, up to 254 L/min), which was coupled to a volumetric container (backwater) to absorb the pressure oscillations in the piston. The volumetric container was followed by a manometer and a rotameter to regulate the air pressure and to measure the flow, respectively. The fresh biomass was lit at the top; therefore, the reaction front went down to the bottom part of the reactor (grate). The reaction front was formed by the stages of drying, pyrolysis, oxidation and reduction. Concerning its geometry, the reactor was cylindrical and had an internal diameter of 0.16 m and a height of 0.28 m. Additionally, there were 5 type-K thermocouples (±1 °C) that were longitudinally located in the reactor and separated every 0.04 m, so that the temperature along the gasification bed was monitored. The 5 thermocouples were inserted 5 mm into the reactor, seeking to avoid air channels in the biomass. Therefore, the

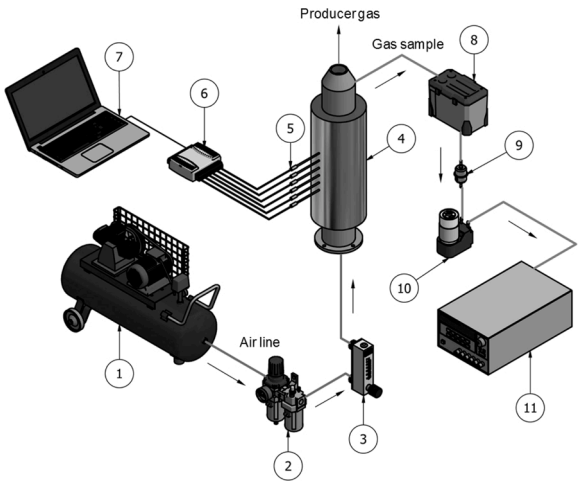

Fig. 1. Experimental setup: 1) reciprocating compressor, 2) filter and flow regulator, 3) air rotameter, 4) insulated fixed-bed gasifier, 5) K-type thermocouples, 6) data acquisition system, 7) computer, 8) gas conditioning, 9) gas filter, 10) vacuum pump, 11) gas chromatograph.

measured temperature inside the bed was near the reactor-wall. The experimental installation had a data control and an acquisition system consisting of a National Instruments USB-6001 device, and a program developed with *LabView*®.

WP and WCH initial mass values for the gasification process were ~1300 g and ~550 g, respectively. This mass variation was ascribed to the higher bulk density of the former biomass with regard to the latter one. Gasification air flow was 146 ± 4.35 L/min (0.12 kg/m^2/s ± 3.58 × 10^{-3} kg/m^2/s), and was fixed for both types of biomass in order to evaluate the effect of the fuel type in the produced BCs. The fuel consumption rate was registered through a *MAG master P* weighing scale with a capacity of 30 kg (±0.1 g), on which the gasifier was set during the experimental test. Finally, the gasification gas composition (*syngas*) was measured by using a *Gasboard-3100 Serial (Cubic-Ruiyi Instrument)* gas analyzer, and it was given in: CO (± 2%vol of FS, by non-dispersive infrared - NDIR), CO_2 (± 2%vol of FS, by NDIR), CH_4 (± 2%vol of FS, by NDIR), H_2 (± 3%vol of FS, by thermal conductivity detector - TCD), O_2 (± 3%vol of FS, by electrochemical detection - ECD), C_3H_8 (± 2%vol of FS, by NDIR), and N_2 (calculated by difference).

The parameters characterizing the gasification process were the process maximum temperature measured near the reactor-wall (T_{max}, °C), the fuel/air equivalence ratio (F_r, dimensionless), the biomass burning velocity (V_b, mm/min), the biomass consumption rate ($\dot{m}_{bms}$, kg/h/m^2), the composition on a dry base (%vol) and the volumetric flow ($\dot{V}_{pg}$, Nm^3/h), as well as the low heating value (LHV_{pg}, kJ/Nm^3) of the producer gas, the cold gas efficiency (CGE, %), the producer gas yield (Y_{pg}, Nm$^3_{pg}$/kg$_{bms}$), and the BC mass yield (Y_{char}, %). F_r (-), LHV_{pg} (kJ/Nm^3), and CGE (%) were calculated following the methodology proposed by Díez et al. (2018). T_{max} (°C) was obtained through the thermocouples located along the reactor. The specific biomass consumption rate, $\dot{m}_{bms}$ (kg/h/m^2), was determined by using Eq. (1).

$$\dot{m}_{bms} = \frac{m_{bms}}{A_T} \tag{1}$$

where m_{bms} (kg/h) is the biomass consumption rate, which corresponds to the slope in the curve between the biomass weight loss registered by the *MAG master P* scale and the time elapsed during the test execution. A_T (m^2) refers to the reactor cross-section (0.0201 m^2). In turn, V_b (mm/min) is the ratio between $\dot{m}_{bms}$ (kg/h/m^2) and the biomass bulk density (ρ, kg/m^3), as expressed in Eq. (2).

$$V_b = \frac{\dot{m}_{bms}}{\rho_{bms}} \tag{2}$$

Y_{pg} (Nm$^3_{pg}$/kg$_{bms}$) was calculated through Eq. (3), which relates the producer gas volumetric flow ($\dot{V}_{pg}$, Nm^3/h) and the biomass consumption rate, m_{bms} (kg/h) (Guo et al., 2014).

$$Y_{pg} = \frac{\dot{V}_{pg}}{m_{bms}} \tag{3}$$

where $\dot{V}_{pg}$ (Nm^3/h) was obtained from N_2 mass balance in the producer gas with regard to N_2 in the air (Lenis et al., 2016). Finally, Y_{char} (%) was calculated from the relation between the BC final mass reached at the end of the test (m_f, kg) and the biomass initial mass (m_{ini}, kg), as described in Eq. (4).

$$Y_{char} = \frac{m_f}{m_{ini}} \tag{4}$$

An analysis of variance (ANOVA) was carried out in order to support the analytical characterization of the achieved BCs and, subsequently, to statistically validate the results obtained. Thereby, the biomass density was considered as the experimental factor with two levels (555.97 kg/m^3 for WP, and 151.29 kg/m^3 for WCH). For this purpose, gasification experimental replicates were carried out for each biomass type (WP and WCH) to accomplish a completely randomized experimental design. The statistical model is presented in Eq. (5), where μ is the global average, τ_i refers to the effect of the *i*-th treatment, and ε_{ij} is the error (Montgomery, 2004).

$$Y_i = \mu + \tau_i + \varepsilon_{ij} \tag{5}$$

The reverse downdraft reactor at lab scale simulates the downdraft gasifiers configuration. According to the information reported in the literature, this technology is able to produce power by internal combustion engines, as well as BC (Estrada et al., 2019; Perez et al., 2015). On the other hand, the power capacity of this technology is able to range from 0.1 to 1.0 MWe, with commercial specific costs between 2000 and 22,000 US$/kWe, which depends on the power plant capacity and supplier (Pérez et al., 2018). It is important to note that the investment required to this kind of bioenergy projects based on renewable resources is driven by tax incentives proposed by the Colombian Renewable Energy Law 1715, such as a) deduction of income tax during the first five years of project operation; b) exemption from VAT on national or imported equipment, machinery, and services for the project; c) exemption from the tax payment of import; and d) accelerated depreciation on assets (Congreso de Colombia, 2014).

2.3. Biochars as solid biofuels

2.3.1. Chemical characterization

The proximate analysis of patula pine WP and WCH, and the derived BCs (WP-BC and WCH-BC) was determined through a *TGA Q50* thermogravimetric analyzer under the ASTM D-5142-04 modified standard (Medic et al., 2012). The moisture content (MC), the volatile material (VM), the fixed carbon (FC) and the AC present in the samples were measured. The ultimate analysis (C, H, N, S, and O contents) for WP, WCH, WP-BC, and WCH-BC was determined using a *Leco Truspec micro* equipment under the ASTM D-5373-08 standard (ASTM, 2008). CHN elemental contents and S content were determined at 1050 °C and 1350 °C, respectively, in a helium (He) atmosphere. In turn, O concentration was estimated by difference (Protásio et al., 2013).

The functional groups on the surface of the four samples were determined through Fourier transform infrared spectrography (FTIR) (Qian et al., 2013). An *IRAffinity-1 (Shimadzu, Japan)* equipment was used along with a detector operated in a range of wavenumbers of 4000 and 400 cm^{-1}. Fang et al. (2014) stated that the main changes in the BC chemical structure were aromaticity and dehydration. Aromaticity index (*A*, dimensionless) was calculated through Eq. (6) (Brewer et al., 2011), where FC (wt%) is the fixed carbon, and VM (wt%) stands for the fuel volatile matter content.

$$A = \frac{FC}{FC + VM} \tag{6}$$

The fibers analyses (lignin, cellulose and hemicellulose) from the raw biomasses and BCs were determined through the *Van Soest AOAC 962.09 and 978.10* method (van Soest et al., 1991v), with a *FiberCap Foss-2022* equipment. The lignin separation was carried out through sulfuric acid (H_2SO_4) at 72 %. Afterwards, acid detergent fiber (ADF) was determined as the sum of cellulose and lignin fibers. Finally, neutral detergent fiber (NDF) was quantified as the sum of the acid detergent fiber and hemicellulose (Ramos-Carmona et al., 2018). Samples were analyzed in triplicate and the method error was 1.2 %.

2.3.2. Physical characterization

The bulk density (ρ, kg/m^3) is defined as the ratio between the mass and the volume occupied by the material particles. In order to measure the referred parameter, a recipient with an internal diameter equal to the gasifier bed diameter (16 cm) was used (Lenis and Perez, 2014). The WP and WCH bulk density measurements were made just as they were entered into the reactor. Meanwhile, for the WP-BC and WCH-BC, bulk density measurements were made as they were produced in the gasification process.

Particle sphericity (φ, dimensionless) is a parameter which allows to identify how similar is the shape of the particles to a sphere. Sphericity has been reported to directly affects biomass packing factor into the bed. On the other hand, the packing factor increased for biomasses with a higher sphericity (Porteiro et al., 2010). This parameter was determined through a ratio between the particle volume and its area. Specifically, WP sphericity was calculated by approximating the geometry to a cylinder of diameter (d, m) and length (L, m), as shown in Eq. (7). For WCH, the geometry was approximated to a flat prism with a width (L_1, m), height (L_2, m), and length (L_3, m). The calculation for the chip sphericity was carried out through Eq. (8) (Díez and Pérez, 2019).

$$\varphi = \frac{d^{\frac{1}{3}}\left(\frac{3}{2}L\right)^{\frac{2}{3}}}{L + \frac{1}{2}d} \tag{7}$$

$$\varphi = \left(\frac{\pi}{L_2}\right)^{\frac{1}{3}} \frac{(6L_1L_3)^{\frac{2}{3}}}{(4L_3 + 2L_1)} \tag{8}$$

The surface area, and the pore size and volume of the four materials (WP, WCH, WP-BC, and WCH-BC) were determined by using an *ASAP 2020* equipment, through adsorption isotherms with N_2. Surface area calculation was carried out by using the *Brunauer, Emmett and Teller* (BET) method, which was applied to the adsorption data of N_2 in the relative pressure interval (P/P_0) 0.05−0.35 to 77 K. Samples were degassed at 10 μmHg for 18 h at a temperature of 80 °C for the raw woods, and 250 °C for the BCs. It is worth noting that 250 °C is lower than the gasification temperature at which BCs were produced. On the other hand, the *Barrett, Joyner and Halenda* (BJH) method was used to determine the pore size and volume (Qian et al., 2013).

The surface morphology of the four samples was observed through a *JEOL JSM-6490* microscope operating at an accelerating voltage of 20 kV. Samples were covered by a gold film before being entered to the equipment and observations were made at a magnification of ×1000.

2.3.3. Energy characterization

The higher heating values (HHV, kJ/kg) of the pine wood biomasses (WP and WCH) and the derived BCs were determined through a calorimetric pump following the ASTM D2015-85 standard (ASTM, 1996). The lower heating value (LHV, kJ/kg) was calculated from HHV and Eq. (9) (Díez et al., 2018), where MC (g/g) and H (g/g) are the moisture and the hydrogen content, respectively, for each fuel.

$$LHV = HHV - 2260 \cdot MC - 20300 \cdot H \tag{9}$$

In turn, the FVI (MJ/cm^3) is the fuel energy density corrected by the ash and moisture contents, which was calculated through Eq. (10) (Díez and Pérez, 2019), where LHV (MJ/kg) is the lower heating value of the solid fuel, ρ (kg/cm^3) is the fuel bulk density, and AC (g/g) and MC (g/g) are the ash and moisture contents of the fuel, respectively.

$$FVI = \frac{LHV \cdot \rho}{AC \cdot MC} \tag{10}$$

The ash mineral composition of the four samples (WP, WCH, WP-BC, and WCH-BC) was measured through an X-ray fluorescence analysis (XRF). The equipment used was a *Thermo ARL Optim'X WDXRF* under the ASTM D4326-94 standard (Vamvuka et al., 2009). The procedure for the test execution consisted of drying the samples for 24 h at 110 °C. Then, the samples were stabilized in a desiccator and calcined at 950 °C. XRF analysis was executed in a He atmosphere at room temperature and for 25 min. The amount of oxides in the ashes, such as CaO, MgO, P_2O_5, K_2O, MnO, SO_3, SiO_2, Al_2O_3, Na_2O, BaO, CuO, TiO_2, Fe_2O_3, NiO, and SrO, was thus determined. Through the ash composition, the indexes related to the properties of deposition and dirtying of the fuels inside the reactors under thermochemical processes like gasification/combustion were determined (García et al., 2015).

Fuel tendency to fuse and make encrustations and slag is related to ash composition determined by using XRF. This tendency was quantified through deposition predictive indexes; among them the alkali index (AI) and the base/acid ratio ($R_{b/a}$) are highlighted (García et al., 2015). AI quantifies how prone a solid fuel to melting or corrosion is. This index expresses the alkali oxide amount in the fuel per unit of energy (alkali kg/GJ) and it was calculated by using Eq. (11) (Bridgeman et al., 2007).

$$AI = \frac{1}{HHV} \cdot AC \cdot (K_2O + Na_2O) \tag{11}$$

where HHV (GJ/kg) refers to the fuel higher heating value, AC (g/g) is the fuel ash content, and K_2O (g/g) and Na_2O (g/g) are the potassium oxide and sodium oxide fractions in the ashes, respectively. As reported in the literature, an AI > 0.17 kg alkali/GJ shows a likely melting, while an AI ≥ 0.34 kg alkali/GJ leads to a certain melting (Jenkins et al., 1998). $R_{b/a}$ is an indicator of the slag or deposition formation tendency, and it was calculated through Eq. (12). Each oxide was expressed as percentage of ash weight (g/g). $R_{b/a}$ is one of the most reported indexes in the literature (Bridgeman et al., 2007; García et al., 2015; Vamvuka et al., 2009). The criterion for establishing deposition existence was found to be in the following ranges: $R_{b/a} < 0.5$ lower, $0.5 < R_{b/a} < 1.0$ medium, and $R_{b/a} > 1.0$ high probability of ash deposition (García et al., 2015).

$$R_{b/a} = \frac{Fe_2O_3 + CaO + MgO + K_2O + Na_2O}{SiO_2 + TiO_2 + Al_2O_3} \tag{12}$$

2.3.4. Devolatilization reactivity analysis

The reactivity analyses under devolatilization of the four samples were conducted under a thermogravimetric analyzer *TGA Q50*. The samples were dried at 105 °C during 24 h before characterization in order to avoid interferences with the drying process in the devolatilization study. The mass quantity per sample was ~10 mg. Each sample was heated from room temperature (~ 25 °C) to 900 °C, at a heating rate of 20 °C/min. The devolatilization process was carried out in an inert atmosphere (N_2) supplying a flow of 120 mL/min. This test allowed to assess the thermal stability of the raw biomasses and the derived BCs based on a thermogravimetric analysis (TGA). Furthermore, it was possible to determine the sample reactivity in order to establish the reaction velocities under devolatilization conditions.

The thermal stability was analyzed through the base temperature (T_{base}), which corresponds to the temperature at which a derivative in the differential thermogravimetric analysis (DTG) equal to 1%/min is reached at the devolatilization stage (Zapata et al., 2014). The sample with the highest base temperature was considered more thermally stable. In addition, the reactivity, *i.e.*, the reaction velocity under

devolatilization conditions was calculated through Eq. (13), where R_a (min^{-1}) corresponds to the reactivity, m_o (mg) is the initial mass of the thermogravimetric analysis, and DTG $_{max}$ (mg/min) stands for the highest value of DTG curve (Ramos-Carmona et al., 2018).

$$R_a = \frac{1}{m_o} \cdot DTG_{max} \quad (13)$$

In this section, the calculation model for determining the stages and the kinetic parameters characterizing the devolatilization process of the raw biomasses, WP and WCH, is described. The objective was to evaluate which of the two types of biomasses is the most reactive for the production of BCs under thermochemical processes. Pyrolysis kinetics was used, which is based on the non-isothermal thermogravimetric analysis (TG) in an inert atmosphere, and on the non-model methods that require the combination of experimental tests at different heating rates (Nzioka et al., 2019). Biomass reactivity was determined through the calculation of the activation energy (E_α, kJ/mol) and the pre-exponential factor (A_α, 1/s).

Devolatilization tests were carried out in a thermobalance *TGA Q50* at different heating rates (βj), 10, 20, 30 and 40 °C/min from 25 °C to 900 °C. The N_2 volumetric flow supplied in each trial was 120 mL/min, and the mass of each devolatilized sample was ~10 mg. This procedure was similar to that one proposed by Bonilla et al. (2019). For each raw biomass (WP and WCH), conversion variation or pyrolyzed mass fraction g(α) was calculated through Eq. (14) as a function of the heating rates (Bonilla et al., 2019).

$$\alpha = \frac{m_i - m_t}{m_i - m_f} \quad (14)$$

where m_i (mg) and m_f (mg) are the initial and the ending mass of the sample, respectively, and m_t (mg) corresponds to the sample mass at an instant of time *t*.

In the current study, devolatilization kinetics was calculated through the model proposed by Santos et al. (2015). For each type of biomass, α was depicted as a function of the temperature (see Fig. A1, Appendix A), in order to establish the range associated with the highest biomass conversion. In this work the biomass conversion interval was $0.2 \leq \alpha_i \leq 0.8$. The activation energy (E_α, kJ/mol) and the pre-exponential factor (A_α, 1/s) were calculated in the range α_i following three methods: Flynn-Wall-Ozawa (FWO), Kissinger-Akahira-Sunose (KAS) and Friedman (Heydari et al., 2015; Kple et al., 2016), which are described by Eqs. (15)–(17), respectively. Isoconversional lines were built for each method for the different conversion grades (α_i), refer to Fig. A2, Appendix A.

$$\ln(\beta_j) = \ln\left(\frac{A_\alpha E_\alpha}{Rg(\alpha)}\right) - 5.331 - 1.052\frac{E_\alpha}{RT_{\alpha_i}} \quad (15)$$

$$ln\left(\frac{\beta_j}{T_{\alpha_i}^2}\right) = ln\left(\frac{A_\alpha R}{E_\alpha g(\alpha)}\right) - \frac{E_\alpha}{RT_{\alpha_i}} \quad (16)$$

$$ln\left(\beta_j \frac{d\alpha}{dT}\right) = ln(A_\alpha f(\alpha)) - \frac{E_\alpha}{RT_{\alpha_i}} \quad (17)$$

where $T_{\alpha i}$ (K) is the conversion temperature to a specific α_i, R (J/K-mol) corresponds to the gas universal constant (8.314 J/K-mol), and β_j (K/min) refers to the heating rate. Functions $g(\alpha)$ and $f(\alpha)$ correspond to the most common reaction mechanisms in solid-state reactions (Liu et al., 2014). According to FWO method, E_α (kJ/mol) was determined through Eq. (18) (Slopiecka et al., 2012).

$$E_\alpha = -\frac{m_{fwo} R T_{\alpha_i}}{1.052} \quad (18)$$

where m_{fwo} is the graph slope ln(βj) *vs.* $1000/T_{\alpha i}$ (Fig. A2a, Appendix A). Concerning the KAS method, E_α (kJ/mol) was calculated by using Eq. (19) (Slopiecka et al., 2012).

$$E_\alpha = -m_{kas} R T_{\alpha_i} \quad (19)$$

where m_{kas} is the graph slope $\ln(\beta j/T^2_{\alpha i})$ *vs.* $1000/T_{\alpha i}$ (Fig. A2b, Appendix A). Finally, according to the Friedman method, E_α (kJ/mol) was estimated through Eq. (20) (Heydari et al., 2015).

$$E_\alpha = -m_{Fried} R T_{\alpha_i} \quad (20)$$

where m_{Fried} is the graph slope $\ln(\beta j \cdot d\alpha_i/dT_{\alpha i})$ *vs.* $1000/T_{\alpha i}$ (Fig. A2c, Appendix A).

The pre-exponential factor (A_α) of the devolatilization reaction of the raw woods was determined through Eq. (21), considering the first-order kinetics hypothesis. As reported in the literature, the referred hypothesis is correct when E_α does not significantly vary with regard to the pyrolyzed mass fraction (α) (Vyazovkin et al., 2011). Where T_m (K) is the temperature corresponding to the highest point of the curve $d\alpha/dT$ *vs.* T , as illustrated in Fig. A3, Appendix A.

$$A_\alpha = \frac{\beta_j E_\alpha}{RT_m^2} exp\left(\frac{E_\alpha}{RT_m}\right) \quad (21)$$

Table 1
Gasification conditions of the raw biomasses (WP and WCH) to produce the derived biochars WP-BC and WCH-BC.

Gasification process parameters	Gasification biochar type	
	WP-BC	WCH-BC
T_{max} (°C)	391.07 ± 81.68	229.70 ± 30.77
V_b (mm/min)	3.73 ± 0.46	16.02 ± 2.17
F_r (-)	1.52 ± 0.19	1.85 ± 0.25
$\dot{m}_{bms}$ (kg/h/m^2)	125.33 ± 15.48	145.39 ± 19.72
Producer gas composition, dry basis (%vol.)		
CO	11.66 ± 1.52	10.02 ± 0.94
CO_2	13.30 ± 0.98	13.51 ± 0.85
CH_4	2.71 ± 0.44	2.3 ± 0.47
H_2	4.78 ± 1.47	1.87 ± 0.90
N_2	66.83 ± 2.41	71.16 ± 1.70
O_2	0.61 ± 0.31	1.03 ± 0.57
C_3H_8	0.10 ± 0.02	0.11 ± 0.02
$\dot{V}_{pg}$ (Nm^3/h)	7.97 ± 0.28	7.48 ± 0.16
LHV_{pg} (kJ/Nm^3)	3047.90 ± 422.94	2384.58 ± 274.06
CGE (%)	51.59 ± 5.09	36.67 ± 4.95
Y_{pg} (Nm$^3_{pg}$/kg$_{bms}$)	3.21 ± 0.35	2.60 ± 0.32
Y_{char} (wt%)	12.12 ± 1.19	10.82 ± 1.24

3. Results and discussion

3.1. Gasification conditions

The operative parameters of WP and WCH gasification process are listed in Table 1, including the maximum temperature of the process (T_{max}, °C), the fuel/air equivalence ratio (F_r, dimensionless), and the biomass burning velocity (V_b, mm/min), which affect BC properties (Qian et al., 2013). Furthermore, the biomass consumption rate ($\dot{m}$ $_{bms}$,

Table 2
ANOVA summary for the gasification parameters as a function of the biomass density (WP and WCH) for the production of WP-BC and WCH-BC.

Response variable	p-value	Significance
V_{ff}	0.0000	Yes
F_{rg}	0.0000	Yes
T_{max}	0.0000	Yes
Y_{char}	0.0016	Yes
Y_{gas}	0.0000	Yes
LHV_{pg}	0.0000	Yes
CGE	0.0000	Yes
V_{bms}	0.0005	Yes
$\dot{V}_{pg}$	0.0000	Yes

Table 3
Physicochemical and energy properties for the raw biomasses (WP and WCH) and the biochars derived from gasification (WP-BC and WCH-BC).

Property	Standard	Raw wood		Biochar	
		WP	WCH	WP-BC	WCH-BC
Proximate analysis dry base (wt%)					
VM	ASTM D5142-04	84.64	83.83	20.59	24.36
FC	By difference	14.09	15.85	77.49	72.90
AC	ASTM D5142-04	1.27	0.32	1.92	2.74
MC (wt%)	ASTM D5142-04	7.91	11.12	11.13	11.63
A (-)	Calculated	0.14	0.16	0.79	0.75
Ultimate analysis dry ash free (wt%)					
C	ASTM D5378-08	47.01	47.38	97.94	97.06
H	ASTM D5378-08	5.69	6.08	0.97	0.85
O	By difference	47.28	46.38	0.9	1.66
N	ASTM D5378-08	0.02	0.16	0.19	0.43
O/C	–	0.75	0.73	0.01	0.01
H/C	–	1.45	1.54	0.12	0.11
Energy properties					
HHV (MJ/kg)	ASTM D2015	20.36	18.34	29.25	28.36
LHV (MJ/kg)	Calculated	19.03	16.85	28.80	27.92
FVI (MJ/cm$^{3)}$	Calculated	10.61	7.12	3.18	0.80
Fiber content (wt%)					
Lignin	–	43.74	39.10	86.00	77.00
Cellulose	–	32.83	35.70	1.69	1.10
Hemicellulose	–	12.73	12.65	1.04	1.51
Physical properties					
ρ (kg/m$^{3)}$	–	559.97	151.29	236.28	91.05
φ (-)	Calculated	0.87	0.70	0.81	0.61
BET (m^2/g)	–	1.16	4.66	367.33	233.56
PV (cm^3/g)	–	0.0006	n.d.	0.20	0.13
Ø (Å)	–	1.95	n.d.	2.19	2.19

n.d.: not detected.

kg/h/m^2), the dry base composition (%vol) and the volumetric flow ($\dot{V}_{pg}$, Nm^3/h), as well as the lower heating value (LHV$_{pg}$, kJ/Nm^3) of the producer gas, the cold gas efficiency (CGE, %), the producer gas yield (Y$_{pg}$, Nm$^3_{pg}$/kg$_{bms}$), and the biochar yield (Y$_{char}$, wt%) are also presented. These parameters support the results obtained from the biomass type effect on the generated BC properties.

ANOVA was used to evaluate the statistical effect of the biomass density on the gasification process parameters. In Table 2, a summary of the results obtained once ANOVA was conducted for a confidence level of 95 % is shown. According to the p-values achieved, it can be observed that the entire set of the response variables evaluated are significant from a statistical point of view, since the associated p-values are below 0.05. Therefore, it can be concluded that the biomass density exerts a significant effect on the biomass gasification process.

Considering that the air flow, it was set at a constant value for both types of biomass, T$_{max}$ in the WP gasification process was ~70 % higher than that one reached by using WCH, with values of 391.07 °C and 229.70 °C, respectively. The highest temperature for WP was due to the higher LHV and bulk density values associated in comparison with the values found for WCH. The heat released inside the bed increased with the superior heating value (19.03 MJ/kg, Table 3), which in turn resulted in the process temperature rise. Moreover, the WP higher density produced an increased packing factor (PF = 0.48) inside the reactor with respect to the PF obtained by WCH (PF = 0.36) (Lenis and Pérez, 2014). As reported in the literature, as the biomass PF increases, the radiative heat transfer penetration in the solid phase decreases, while the absorption of this heat transfer mechanism increases (Lenis et al., 2016; Perez et al., 2015; Shin and Choi, 2000). On the other hand, it is important to note that a higher radiation intensity absorption caused an increase in the energy concentration in the reaction front, which led to a rise in the process temperature reached for WP. Despite the lower temperature for WCH, the biomass burning rate (V$_b$) of WCH was 4.3 times higher than that one reached by WP. This behavior was due to the higher radiative heat transfer penetration in the solid phase of WCH, whose mechanism favored the biomass drying and devolatilization processes, resulting in a higher reaction velocity in the gasification process (González et al., 2018; Perez et al., 2015). Likewise, the biomass consumption rate was ~16 % higher for WCH, with values of 145.39 kg/h/m^2 compared to 125.33 kg/h/m^2 for WP. The trend found for $\dot{m}_{bms}$ was similar to that one observed for V$_b$, since both variables are correlated (Eq. (2)) (González et al., 2018). Therefore, due to higher biomass consumption rates were enhanced by the high radiative heat transfer penetration in WCH, F$_r$ increased by ~22 % for WCH with regard to the F$_r$ for WP (Lenis et al., 2016; Perez et al., 2015; Shin and Choi, 2000).

In this study, it is highlighted a divergent effect between the fuel/air equivalence ratio (F$_r$) and the gas composition for these two types of biomass. Although F$_r$ for WP was 1.52 (slight fuel-rich reaction) and for WCH was 1.85 (higher fuel-rich reaction), a high concentration of gaseous fuels was found for WP, whose composition was 16 %, 18 % and 155 % higher for CO, CH_4 and H_2, respectively, compared to the gas composition obtained when WCH was used. The higher concentration of gaseous fuels produced by WP caused an increase of ~28 % in LHV$_{pg}$, with values of 3047.90 kJ/Nm^3 for WP, and 2384.58 kJ/Nm^3 for WCH. This effect can be attributed to the higher reaction temperature reached for WP, which favored the reduction reactions and, thus, the generation of fuel gaseous species (Erlich and Fransson, 2011). On the other hand, the producer gas volumetric flow ($\dot{V}_{pg}$) reached by WP was 7% higher than that one obtained for WCH, with values of 7.97 Nm^3/h and 7.48 Nm^3/h, respectively. The increased producer gas yield for WP was ascribed to its higher bulk density (559.97 kg/m^3, Table 3), which increased the biomass amount per unit of reactor volume, favoring the gas production due to the mass conservation. Regarding the cold gas efficiency (CGE), the obtained values were 51.6 % for WP and 36.7 % for WCH. The difference of ~41 % could be due to the higher flow and LHV$_{pg}$ of the producer gas reached for WP, as well as to the low biomass consumption rate (16 %) achieved for WP. Therefore, the energy supplied by the WP biomass to the gasification process was reduced while CGE was increased.

Finally, the producer gas and the biochar yields were higher for WP. Y$_{pg}$ was 23 % higher for WP in comparison with the value found for WCH, since WP showed a higher gas volumetric flow (~6%) and a lower biomass consumption rate (~16 %). On the other hand, the value corresponding to Y$_{char}$ for WP was 12.12 %, while that one for WCH was 10.82 %. The higher biochar yield for WP was attributed to the biofuel higher bulk density (González and Pérez, 2019). Furthermore, the biomasses with a higher lignin content have been reported to tend to produce a higher biochar yield (Sohi et al., 2010); in this case, the lignin content for WP was ~12 % higher than that one for WCH (Table 3).

3.2. Biochar chemical properties

3.2.1. Proximate analysis

The proximate analyses for the raw biomasses and the BCs are shown in Table 3. The VM contents for WP and WCH were 84.64 wt% and 83.83 wt%, respectively. These results show that the gasification of both types of biomasses was favored due to their amount of thermally degradable compounds (Ceylan and Topçu, 2014; Pérez et al., 2019). In turn, the VM content for the BCs show an average reduction by 73 % compared to the VM content of the raw biomasses, with values of 20.59 wt% and 24.36 wt% for WP-BC and WCH-BC, respectively. This depletion can be the result of pyrolysis, oxidation, and reduction reactions occurring during the gasification process, where the VM content present in the raw material was transformed in the producer gas. Comparing both BCs, the VM content for WP-BC was 15.5 % lower than that of WCH-BC; which can be attributed to the higher temperature reached during WP gasification in comparison with the temperature achieved when WCH was transformed, favoring the thermal degradation of hemicellulose and cellulose (Ramos-Carmona et al., 2018), and thus, enabling the production of a carbonaceous solid primarily formed by lignin (González et al., 2018). This composition was related to the average content of the

fixed carbon (FC), which was ~5 times higher for BCs. For WP-BC, the FC was 6% higher than that of WCH-BC due to the higher lignin content of the WP, and the higher gasification temperature (Lv et al., 2010).

On the other hand, the AC values of the raw biomasses were within the range for lignocellulosic biomasses (< 2.5 wt%) (Díez and Pérez, 2017). Such amount of inert material promotes the production of BCs with a lower AC, and thus the heating value of the solid byproduct is not adversely affected (Ceylan and Topçu, 2014). The WP AC was 1.27 wt% with regard to 0.32 wt% for WCH, this difference might be ascribed to the slight thermal pretreatment produced during the WP densification process (González et al., 2020). In turn, the AC values for WP-BC and WCH-BC were 1.92 wt%, and 2.74 wt%, respectively. This relative increase in AC for the studied BCs was ascribed to the thermal degradation of the biomass constituents (hemicellulose and cellulose) during gasification (Wang et al., 2014). Therefore, the BCs obtained from patula pine (WP and WCH) gasification are suitable to be used as solid biofuels in thermochemical processes due to their appropriated AC (< 25 wt%) (Lapuerta et al., 2008).

The difference in MC between WP-BC and WCH-BC was found to be lower than 5%. However, with respect to the raw biomasses, MC increased by 41 % and 5% for WP-BC and WCH-BC, respectively. Despite the MC values for both BCs were < 12 wt%, the increase in MC could be attributed to the water vapor coming from the oxidation reactions of the gasification process, whose vapor is condensed in the carbonaceous solid matrix due to the gasification stages configuration into the reverse downdraft reactor (Tinaut et al., 2008).

3.2.2. Ultimate analysis

The results from the ultimate analysis on dry ash-free base for the four materials are shown in Table 3. It is worth noting that the C content in BCs was ~2.1 times higher with regard to the raw biomasses. This can be explained by the temperatures associated with the gasification process, which favor the biomass reaction mechanisms (*e.g.*, drying, devolatilization, oxidation and reduction) (Jindo et al., 2014). Therefore, the average FC of the obtained BCs was ~5 times higher and, as a consequence, the C content increased. H and O contents of the generated BCs decreased on average by 85 % and 97 %, respectively. This reduction can be due to the thermochemical degradation of the hemicellulose and the cellulose (James et al., 2016). In turn, the N content was observed to increase in the produced BCs, even though the mass fraction of this elemental component was lower than 1.0 wt%.

3.2.3. FTIR - functional groups

FTIR spectra for the studied materials are represented in Fig. 2. The aromaticity index (Eq. (6), Table 3) was ~5.0 times higher for the obtained BCs with regard to that one for the raw biomasses, showing that BCs are products of the functional groups losses related to OH and CH bands. The region between 3700 cm^{-1} and 3000 cm^{-1} corresponds to the stretching of —OH, water molecules, hydroxyl groups (OH), and phenols (Qian et al., 2013). The depletion of this peak in BCs can be ascribed to the release of MC and VM from the raw wood samples. The highest intensity of the —OH band exhibited by WCH-BC compared to that one of WP-BC can be attributed to the higher MC in WCH and in the derived WCH-BC (Table 3). Peaks between 2980 cm^{-1} and 2800 cm^{-1} are associated with symmetrical stretching in CH_2 and CH_3 aliphatic compounds, which are typical from materials containing hemicellulose and cellulose (Liu et al., 2011). The lower intensity found in these peaks for the derived BCs was mainly due to the thermal degradation of these constituents (Table 3).

Peaks between 1800 cm^{-1} and 1600 cm^{-1} are linked to the stretching of C═O rings (attributed to hemicellulose), to the vibrations in the aromatic ring of lignin (C═C) (Jindo et al., 2014), and to the bending modes in the —OH plane (associated with the presence of water, oxygenated hydrocarbons and alkyl functional groups) (Díez and Pérez, 2019). These peaks were not found in BCs spectra due to drying and pyro-combustion of the raw biomasses during the gasification process. These gasification stages, where biomass constituents are thermally degraded, might explain the drastic

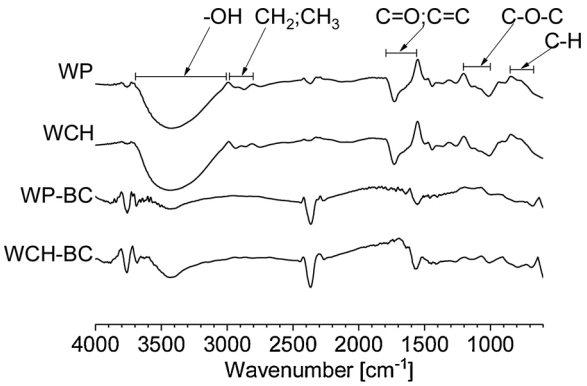

Fig. 2. FTIR spectrum for wood pellets (WP), wood chips (WCH), wood pellets-derived biochar (WP-BC) and wood chips-derived biochar (WCH-BC).

reduction of the peaks observed between 1200 cm^{-1} and 1000 cm^{-1} in the generated BCs, which correspond to the C—O—C stretching associated with the hemicellulose and cellulose contents (Qian et al., 2013). In BCs, the formation of an aromatic structure due to the reduction of the peak at 1520 cm^{-1} associated with the stretching of the C═C ring was observed, as well as the vanishing of the peaks between 850 cm^{-1} and 650 cm^{-1}, caused by the aromatic deformation of C—H (Díez and Pérez, 2019; Liu et al., 2014). Therefore, the BCs studied here are materials that are mainly composed of lignin, which is linked to a high energy density due to the ether bindings and C—C, resulting in a higher energy in comparison to C—O and C—H bindings (Lee et al., 2012). Thereby, BCs reached a heating value of ~58 % higher than that one found for the raw biomasses.

3.2.4. Fiber content

The results for the lignocellulosic content are listed in Table 3. Hemicellulose, cellulose and lignin amounts for WP and WCH were similar since the same forest species was used. The fiber contents for the raw woods were found to be between the reported intervals for these materials (Lv et al., 2010; Ramos-Carmona et al., 2018); besides, a trend in which lignin > cellulose > hemicellulose was observed. According to the literature, hemicellulose and cellulose are mainly associated with the VM content, while lignin mainly favors the BC formation (Lv et al., 2010). Comparing the obtained BCs with the raw biomasses, average reductions by ~90 % and by ~96 % were obtained in the hemicellulose and cellulose content, whilst the lignin content increased by ~97 %. Thus, the high lignin content of BCs can be attributed to the hemicellulose and cellulose degradation during the gasification process, which occurs between 200 and 400 °C (Sikarwar et al., 2016), favoring CO, H_2, CO_2, H_2O and CH_4 production in the producer gas (Montoya et al., 2017). Concerning the lignin content in the generated BCs, it matched the results obtained in the FTIR and proximate and ultimate analyses, where the BCs studied here were found to be biofuels formed primarily by lignin. Therefore, it can be withdrawn that the BC (a rich lignin material) promotes the formation of gaseous fuels (H_2 and CO) under gasification conditions, providing a higher heating value to its producer gas (Dunnigan et al., 2018).

3.3. Physical properties

3.3.1. Bulk density and sphericity

The bulk density and the particle sphericity are relevant properties of solid fuels to make them suitable and useful in thermochemical processes. These properties affect the biomass burning velocity and, therefore, the fuel consumption rate (Lenis and Pérez, 2014). The raw material mass loss (WP and WCH) during the stages of drying, pyro-combustion and gasification produce a BC with low bulk density compared to the raw biomasses (Daniel et al., 2014). Therefore, the reduction in the BC bulk density in comparison with the raw biomasses

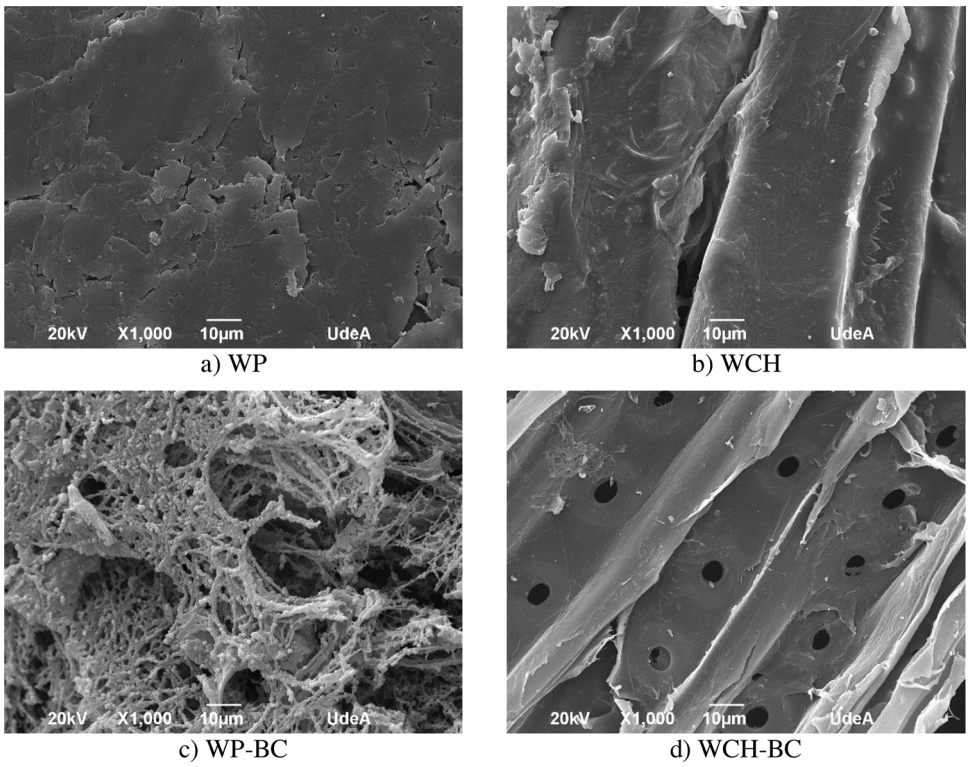

Fig. 3. SEM imaging with a 1000x zoom for a) WP, b) WCH, c) WP-BC and d) WCH-BC.

was by ~58 % and ~40 % for WP-BC and WCH-BC, respectively. Sphericity showed a similar trend, which was reduced by ~7% for WP-BC and by ~13 % for WCH-BC with regard to those ones observed for the raw biomasses. As the temperatures reached in the gasification process favored the hemicellulose and cellulose degradation, the density of the obtained BCs was reduced due to the lower VM content that led to the generation of pores in the structure of the studied BCs; and therefore, an increase in the surface area. On the other hand, the sphericity reduction caused by the variations in the particle size and geometry after the gasification favors the reduction of the PF of BCs in the reactor (Ramos-Carmona et al., 2017). Thereby, when BCs are used as fuel for thermochemical processes in fixed bed technologies, their low sphericity could improve the radiative heat transfer through the solid phase towards the drying and devolatilization stages, leading to a possible increase in the BC burning velocity (Porteiro et al., 2010).

3.3.2. *BET surface area*

The surface area (BET) for the biomasses and BCs studied in this work are presented in Table 3. The difference in the surface area between the evaluated BCs and the raw biomasses was ~97 %. The morphologic and structural changes on the surface of the obtained BCs are largely affected by the high temperatures of the gasification process (700–800 °C) (Guerrero et al., 2005), which promote the release of VM contained in the biomasses, producing a porous structure with a low bulk density (González and Pérez, 2019). Furthermore, during the gasification process two phenomena are presented in the generated BCs: i) the opening of closed pores, and ii) the widening of open pores; therefore, the surface area increases due to the rise of both the number of pores and their average radius (Hernández et al., 2016). The highest BET surface area was found for the WP-BC, with a value of 367.33 m^2/g; this value shows a surface area ~57 % higher than that one of WCH-BC (233.56 m^2/g). The difference between the BET surface areas of the studied BCs was attributed to the higher reaction temperature, which increased when WP were gasified (391.07 °C) instead of WCH (229.7 °C). As analyzed in section 3.1, as the reaction temperature increases in the gasification process, the thermal degradation of the biomass constituents (hemicellulose and cellulose) is favored. This can be ascribed to the breaking of aliphatic compounds of alkyl and ester, and to the lignin core exposition at high temperatures (Chen and Chen, 2009). It is worth noting that the pore structure and the surface area are useful properties to infer access likelihood of reactive gases to the BC internal surface and to the active sites in processes under thermochemical regimes (Qian et al., 2014). Therefore, BCs may have higher gasification reactivity in comparison with other biofuels with less porous structures (Lv et al., 2010); nevertheless, regarding reactivity, the VM content was also observed to be essential (refer to section 3.5).

3.3.3. *Structural analysis through SEM imaging*

Surface morphology for the raw biomasses and their BCs is represented in SEM images, as illustrated in Fig. 3. In Fig. 3a an agglomerated surface of WP ascribed to the lignin is observed, which might be attributed to its mechanical densification pretreatment (González et al., 2020). In contrast, WCH (Fig. 3b) have a fibrous structure, typical of lignocellulosic biomasses (Nanda et al., 2013). In Fig. 3c and d corresponding to WP-BC and WCH-BC, respectively, a carbonaceous structure is illustrated. The carbonaceous structure is ascribed to the hemicellulose and cellulose degradation during the gasification process, remaining a lignin-rich material. A porous amorphous structure was observed for WP-BC due to its production process (Fig. 3c), which consisted of WP (sawdust densification) gasification at high reaction temperatures. For WCH-BC (Fig. 3d), a fibrous structure is still observed, exhibiting open pores along the fibers. The results obtained for WP-BC, regarding to a high BET surface area and a high pore diameter (Table 3) were in agreement with the surface morphology observed through SEM imaging. The pore volume of WP-BC was 54 % higher than that one for WCH-BC; this result is consistent with the higher temperature (~70 % higher) reached during WP gasification. It is expected that the change in the microstructure for the derived BCs promotes a suitable thermal behavior because the high porosity in solid fuels leads to improve the heat and the mass transfer mechanisms in gasification and combustion processes (Ramos-Carmona et al., 2018).

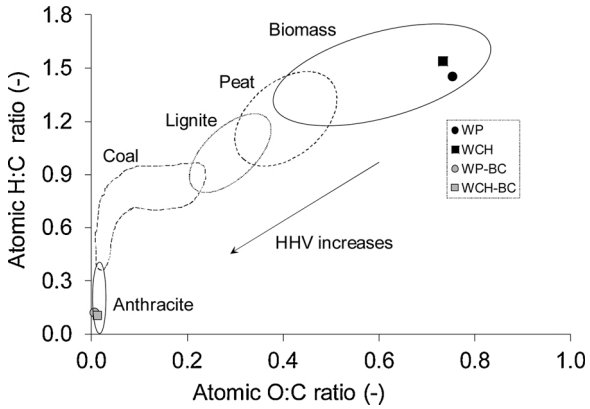

Fig. 4. Van Krevelen diagram for WP, WCH, WP-BC and WCH-BC.

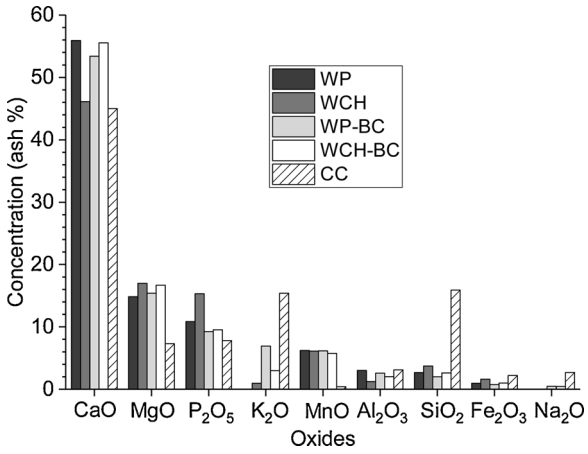

Fig. 5. Ash mineral content of WP, WCH, WP-BC, WCH-BC, and charcoal -CC- (García et al., 2015) as a reference.

3.4. Energy properties

3.4.1. Heating value

In Table 3, the HHV and LHV results for the studied materials are presented. The LHV of WP was ~13 % higher than that one of WCH, in spite of the raw materials come from pine patula wood. However, during the WP densification process, there are some variables involved such as the densification pressure and temperature, which affect the densified biomass properties (González et al., 2020). It is observed that the WP showed a lower MC and H contents, as well as a higher lignin content; these properties favored an increase in LHV. In average, BC LHV was ~58 % higher as compared to those ones of the raw biomasses. This result can be ascribed to the higher lignin content of BCs; since lignin has been reported to have ~30 % more energy content than those ones for hemicellulose and cellulose (Novaes et al., 2010). Additionally, a lower AC in the biomasses favored the higher LHV achieved in the generated BCs. The mild difference of 3% between the LHV of BCs can be explained by their higher contents of FC, C and lignin, which favored the LHV obtained. The HHV of WP-BC and WCH-BC reached values of 29.25 MJ/kg and 28.36 MJ/kg, respectively. Both are comparable to coals, whose values range between 25 and 30 MJ/kg (Ilyushechkin et al., 2014) and to the pine BC heating value (27.46 MJ/kg) obtained by Díez and Pérez (2019). Therefore, the applicability of both BCs as biofuels is remarkable for thermochemical processes, where improvements in their global efficiency are inferred by using BCs with high energy content as a feedstock (Ramos-Carmona et al., 2017).

3.4.2. Fuel value index

The highest FVI (Eq. (10)) was found for WP, 10.61 MJ/cm^3 (Table 3), which represented an energy density (~49 %) higher than that one of WCH (7.12 MJ/cm^3). This result can be mainly ascribed to the largest heating value and high bulk density of WP. Nevertheless, the reduction in the raw biomass bulk density after the gasification process (section 3.3) produced a decrease in the BCs FVI, whose average drop was ~78 %. Regarding WCH biomass, WCH-BC FVI was reduced by ~89 %, which is attributed to the fact that the increase in BC LHV (66 %) does not compensate the reduction in the bulk density (~40 %), nor the increase in the MC (~5%) nor the AC (8.6 times more AC for WCH-BC). Despite the fact that BCs present lower FVI values with regard to the raw biomasses, these materials can be considered as suitable solid biofuels for thermochemical processes due to the considerably high heating value and low AC (Ok et al., 2016).

3.4.3. Van Krevelen diagram

Van Krevelen diagram allows to compare solid biofuels as biomass and BCs with fossil solid fuels as a function of their C, H and O contents (Fig. 4). H/C and O/C atomic ratios are shown in Table 3. WP and WCH had values in accordance with the results reported for lignocellulosic materials, with a typical H/C ratio of ~1.5 (Lehmann and Joseph, 2009). The location of biomasses in the Van Krevelen diagram corresponded to the lowest C content and the highest H and O contents (ultimate analysis, Table 3), which explains the low heating value of the raw biomasses (Nanda et al., 2013).

Nevertheless, H/C and O/C ratios of the obtained BCs showed an average reduction by ~92 % and ~99 %, respectively, with regard to the values found for the raw biomasses. This depletion in BCs can be due to the loss of aliphatic compounds CH_2 and CH_3, and the reduction in oxygenated compounds during the gasification process (section 3.2), which led to the formation of a carbonaceous material mainly constituted of lignin (González et al., 2018). Thus, WP-BC and WCH-BC heating value increased (Pérez et al., 2019), placing them in the region corresponding to the coals (anthracite), whose heating value ranges between 26.0 and 35 MJ/kg (Lv et al., 2019). From Table 3, it is highlighted that BCs derived from WP and WCH were observed to have chemical and energy properties similar to those ones of anthracite (Zha et al., 2016); though, coal anthracite is little reactive; therefore, a higher energy demand is required to initiate reactions in thermochemical processes, while BCs have a higher reactivity due to their hemicellulose and cellulose contents, as well as their surface area. These characteristics highlight the suitable properties of WP-BC and WCH-BC to be used as solid biofuels in thermochemical processes.

3.4.4. Deposition and melting ash

Ash fusion (slag) and fouling are two phenomena related to the equipment deposition and corrosion, which is commonly observed in the biomass combustion systems. Deposition occurs in high temperature zones, generally in the grates and on the reactor walls. As for the melting fouling, it is presented in low temperature zones such as the surfaces near the heat exchangers. The occurrence of these phenomena depends on the fuel chemical composition, the thermochemical transformation technology and the process conditions. Deposition occurs more feasibly when there are high concentrations of elements with low fusion points, such as alkali, sulfides and chlorides (Na, K, S and Cl), while the presence of calcium or magnesium (Ca and Mg) silicates reduces the probability of ash fusion (García et al., 2015). Herein, the ash composition (oxides) of WP, WCH, WP-BC and WCH-BC was compared to the charcoal (CC) obtained from the wood pyrolysis, which is commonly used as a fuel in the combustion process (García et al., 2015).

Fig. 5 presents the chemical composition of the ashes, determined through XRF analysis for the raw biomasses, BCs and CC, in absolute base and without pondering ignition losses. Compounds identified in the ashes are among those ones reported in the literature, where it was explained that lignocellulosic biomasses have higher contents of Ca, Si, P and K, while the levels of Al, Fe and Ti are generally lower (Teixeira et al., 2012). Lignocellulosic biomasses stand out for their high content

Table 4
Indexes of deposition and melting fouling for WP, WCH, WP-BC, WCH-BC and CC.

Method	WP (this work)	WCH (this work)	WP-BC (this work)	WCH-BC (this work)	CC (García et al., 2015)
AI [kg alkali/GJ]	0.00	0.00	0.05	0.03	0.36
$R_{b/a}$	14.50	16.26	18.87	18.33	3.80

of Ca (Zhang et al., 2008), as noted in the four materials studied in this work and in CC (García et al., 2015), while Na is reported as the element with the lowest concentration. Calcium oxide (CaO) content for WP, WCH, WP-BC, WCH-BC, and CC, varied between 46.13 % and 55.91 %. This result can be due to the inorganic compound vaporization (except Ca), because of the high temperatures reached during the gasification process (700–800 °C) (Maiti et al., 2006). It is worth noting that Ca favors the applicability of the four materials as solid biofuels since this chemical element reduces the deposition tendency, preventing agglomeration and ash adhesion to the reactor walls and the heat exchangers (Martínez-Ángel et al., 2015).

The difference between the composition of the raw biomass ashes and BCs was not significant. This indicates that the gasification conditions analyzed in this work did not have an effect on the mineral content of the ashes from patula pine. An increase of the K content was detected for WP-BC and WCH-BC, being WP-BC the one with the highest increase because WP have a higher residence time in the reactor due to a lower burning velocity. K associated with Si may favor the formation of potassium silicates, which exhibit lower fusion temperatures. However, the percentages found in this work were still below the issue threshold, and the potassium silicate effects could be inhibited by the high content of Ca (Teixeira et al., 2012). In comparison with CC, the low content of K and Si exhibited by WP-BC and WCH-BC is highlighted. Their amount of K and Si was about 6 times lower than that one for CC, which may provide good properties to the materials characterized here to be used as solid fuels.

AI and $R_{b/a}$ of the four materials and the reference CC are shown in Table 4. Values for AI were well below to the 0.17 kg alkali/GJ limit, for WP, WCH, WP-BC, and WCH-BC. Therefore, both raw biomasses and BCs would not show risk of corrosion when used as solid fuels. While CC reached an AI of 0.36 kg alkali/GJ (high probability of fouling) due to its high K and Na contents (Fig. 5). On the other hand, the values for $R_{b/a}$ were > 1.0 indicating a deposition probability for the five materials. Nevertheless, Teixeira *et. al* (2012) reported that temperatures at which the ash fusion is started, named as initial deformation temperature, in the case of wood and coal pellets was ~1230 °C and 1200 °C, respectively. This indicates that during the WP and WCH gasification process carried out here, such as temperatures were not reached, as noted on the SEM images (section 3.3) where no ash fusion was observed.

3.5. Devolatilization reactivity analysis

3.5.1. TGA and DTG analysis

Another parameter used to evaluate the solid biofuels behavior was the devolatilization kinetics since the thermal degradation of these materials involves complex chemical reactions (Lee et al., 2017). As shown in Fig. 6a, the raw biomasses (WP and WCH) had a similar profile of mass loss because both samples corresponded to patula pine biomass and were similar with regard to the proximate analysis (Table 3). WP and WCH exhibited several stages in the TG curve. The first stage corresponded to temperatures between 100 °C and 200 °C, in which there was not a significant change in the mass percentage. According to Bonilla et al. (2019) this behavior is due to the formation of chains with cellulose molecules on most of the lignin and hemicellulose molecules, which do not allow the devolatilization of hemicellulose nor cellulose at these temperatures. A second stage took place in the range between 250 °C and 400 °C where most of the mass loss occurs due to hemicellulose (250 °C – 330 °C) and cellulose (330 °C and 400 °C) thermal degradation (Xie et al., 2013). The third stage corresponded to a slow mass loss above 400 °C due to the degradation of lignin and other compounds with stronger chemical bonds (Nyakuma et al., 2015).

BCs showed a lower mass loss in the TG curves (Fig. 6a) because during the gasification process, temperatures close to the reactor wall were between 200 °C and 480 °C, which indicates that the process reached higher temperatures than those values inside the reactor. Consequently, the thermal degradation of WP and WCH constituents was favored as noted in section 3.2. In Table 3, the hemicellulose and cellulose content for the evaluated BCs was lower than 1.70 wt%, while the average lignin content was ~82 wt%. Therefore, the lower mass loss for the BCs was ascribed to the low lignin degradation in the range of temperatures between 160 °C and 900 °C as found by Arteaga-Pérez et al. (2015). A higher mass loss was observed for WCH-BC due to the presence of ~18 % more VM content and ~6% less FC content when compared to WP-BC. Thermal stability of BCs makes them less reactive than the raw biomasses. Therefore, a lower consumption of fuel (biochar) is inferred in thermochemical processes of energy generation due to the low reaction velocities (Misginna and Rajabu, 2014).

DTG curves shown in Fig. 6b confirm that hemicellulose, cellulose and lignin structures are different for raw biomasses and BCs. This behavior was proven through fiber analysis (section 3.2). In WP and WCH, a shoulder was observed at an approximated temperature of 330 °C, which corresponded to the hemicellulose decomposition (Pérez et al., 2019). Additionally, a main peak at 370 °C was observed, which can be attributed to the cellulose degradation (Chen and Kuo, 2010). According to the results reported in Table 5, WP and WCH biomasses have a higher reactivity with regard to their BCs. The base temperature for the raw biomasses was found at ~241 °C, while the BCs do not show T_{base} because maximum peaks of the derivative for BCs were < 1 wt%/min, as observed in Fig. 6b. A lower base temperature is associated with a lower thermal stability or a higher reactivity (Ramos-Carmona et al., 2018). This behavior is directly

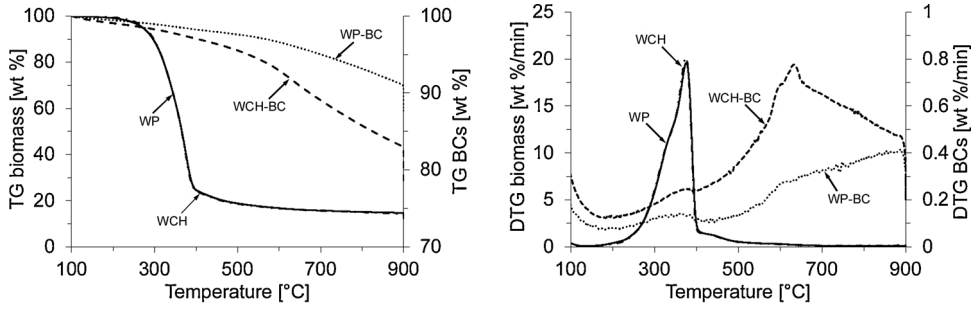

Fig. 6. Thermogravimetric analysis for WP, WCH, WP-BC and WCH-BC.

Table 5
Base temperature (T_{base}) and reactivity for WP, WCH, WP-BC and WCH-BC.

Parameter	WP	WCH	WP-BC	WCH-BC
T_{base} [°C]	239	242	not detected	not detected
R_a [min^{-1}]	0.196	0.202	0.004	0.008

related to the VM content. The raw biomasses resulted to have a similar VM content (Table 3), which caused a slight variation (~3 °C) between both T_{base} values. Nonetheless, after gasification, the average VM content was reduced by ~73 %, significantly reducing reactivity of these carbonaceous materials, and thereby the defined limit in section 2.3.4 to determine T_{base} was not reached.

Another indicator of reactivity under devolatilization regimes is the maximum peak in the DTG curve. The raw biomasses were observed to reach a maximum peak at 370 °C (Fig. 6b), while WCH-BC and WP-BC showed maximum values at 630 °C and higher than 900 °C, respectively. Maximum peaks occurring at lower temperatures show a higher capacity of biofuels to release VM from their structures, indicating a higher reactivity (Zapata et al., 2014). On the other hand, values calculated for R_a were ~97 % lower for BCs. This means that WP-BC and WCH-BC are biofuels with a low reactivity due to the high content of FC and lignin, which is thermally more stable than cellulose (Lv et al., 2010). Thus, reactivity in BCs was slower, which enabled them to require a higher activation energy for VM release, even though their BET surface area is higher (Table 3).

3.5.2. *Pyrolysis kinetics of the raw biomasses*

In this section the pyrolysis kinetics of the raw biomasses (WP and WCH) is characterized. The aim was to assess and compare the WP and WCH reactivity to produce BC under thermochemical processes by means of the kinetic constant determination. Gasification kinetics for the evaluated BCs will be studied in a future work. The results found by Fynn-Wall-Ozawa (FWO), Kissinger-Akahira-Sunose (KAS), and Friedman methods for E_α showed variations lower than ~8% among them. Resemblance among the results indicates standardization, reliability and applicability of the three methods for the kinetic parameters estimation (Bonilla et al., 2019). The average E_α determined values for WP from FWO, KAS and Friedman models were 125.38 kJ/mol, 125.42 kJ/mol and 122.35 kJ/mol, respectively, while those ones for WCH were lower, reaching values of 84.81 kJ/mol, 78.30 kJ/mol and 79.41 kJ/mol, respectively. In each model, R^2 was higher than 0.98, which indicates a good fit of the experimental data (Sobek and Werle, 2020).

E_α did not show meaningful changes regarding α, as noted by the variation lower than 5.5 kJ/mol (see Table 6); consequently, there is a high probability for the pyrolysis reaction to occur in one step (Sobek and Werle, 2020). The results found for E_α of WP and WCH match those ones reported in the literature, such as 168.58–179.29 kJ/mol for pine residues (Mishra and Mohanty, 2018), and 75–130 kJ/mol for agricultural residues (Aboyade et al., 2011; Biagini et al., 2008). Here, E_α for WP was ~54 % higher than that one for WCH, with average values of 124.38 kJ/mol and 80.84 kJ/mol, respectively. This variation can be attributed to the high lignin content and low BET surface area of WP, which give them a higher thermal stability (Lv et al., 2010). Nevertheless, the difference between WP and WCH stems from their physical nature. As previously noted, WP correspond to densified patula pine wood and, for this reason, there were structural changes during the densification process (section 3.3), which provide the biofuel with a higher density. Consequently, as demonstrated in the gasification process, WP had a lower biomass burning rate (V_b) as compared to WCH (section 3.1). This behavior in the gasification parameters was related to E_α, since it has been reported that as E_α increases, the breaking velocity among the chemical bonds decreases (because a higher reaction temperature is required), which leads to a low reactivity and a low reaction velocity of fuels under thermochemical processes (Gai et al., 2013).

On the other hand, the pre-exponential factor for WP varied between 1.30×10^8 s^{-1} and 2.13×10^8 s^{-1}, while the range for WCH was

Table 6
Results of activation energy (E_α), pre-exponential factor (A) and R^2 of linear regressions from Figure A 2, for WP and WCH calculated through the FWO, KAS and Friedman methods.

Biomass	WP						WCH					
Method	FWO			KAS			Friedman			FWO			KAS			Friedman		
α	E_α [kJ/mol]	A [s^{-1}]	R^2	E_α [kJ/mol]	A [s^{-1}]	R^2	E_α [kJ/mol]	A [s^{-1}]	R^2	E_α [kJ/mol]	A [s^{-1}]	R^2	E_α [kJ/mol]	A [s^{-1}]	R^2	E_α [kJ/mol]	A [s^{-1}]	R^2
0.20	118.79	5.05×10^7	0.977	119.40	5.68×10^7	0.974	116.74	3.40×10^7	0.989	72.20	5.03×10^3	0.919	66.64	1.67×10^3	0.906	70.26	3.43×10^3	0.977
0.25	121.57	8.68×10^7	0.991	122.11	9.63×10^7	0.991	119.18	5.47×10^7	0.996	77.43	1.41×10^4	0.953	71.64	4.50×10^3	0.945	75.12	8.96×10^3	0.984
0.30	122.32	1.01×10^8	0.997	122.72	1.09×10^8	0.996	117.54	3.99×10^7	0.998	80.29	2.49×10^4	0.965	74.31	7.64×10^3	0.960	77.52	1.44×10^4	0.970
0.35	122.69	1.08×10^8	0.998	122.94	1.14×10^8	0.998	120.73	7.42×10^7	0.999	83.01	4.24×10^4	0.972	76.86	1.26×10^4	0.967	77.90	1.55×10^4	0.975
0.40	124.73	1.61×10^8	0.999	124.94	1.68×10^8	0.998	121.98	9.47×10^7	0.998	84.24	5.40×10^4	0.974	77.94	1.57×10^4	0.970	78.45	1.73×10^4	0.977
0.45	125.21	1.77×10^8	0.999	125.31	1.81×10^8	0.999	122.60	1.07×10^8	0.997	85.95	7.57×10^4	0.978	79.50	2.13×10^4	0.974	79.28	2.04×10^4	0.977
0.50	127.25	2.63×10^8	0.999	127.33	2.67×10^8	0.999	125.74	1.96×10^8	0.999	86.43	8.32×10^4	0.980	79.84	2.28×10^4	0.976	82.03	3.51×10^4	0.978
0.55	127.51	2.77×10^8	0.999	127.47	2.75×10^8	0.999	125.50	1.88×10^8	0.997	87.19	9.68×10^4	0.980	80.48	2.60×10^4	0.976	81.42	3.12×10^4	0.984
0.60	127.42	2.73×10^8	0.999	127.27	2.65×10^8	0.999	126.28	2.19×10^8	0.998	88.11	1.16×10^5	0.983	81.28	3.04×10^4	0.980	79.88	2.31×10^4	0.986
0.65	127.17	2.61×10^8	0.999	126.90	2.48×10^8	0.999	126.91	2.48×10^8	0.999	88.06	1.15×10^5	0.983	81.13	2.96×10^4	0.980	80.28	2.50×10^4	0.988
0.70	129.00	3.72×10^8	0.999	128.73	3.53×10^8	0.999	127.03	2.54×10^8	0.996	89.13	1.42×10^5	0.983	82.10	3.58×10^4	0.980	80.84	2.80×10^4	0.979
0.75	128.67	3.50×10^8	0.999	128.29	3.25×10^8	0.998	124.17	1.46×10^8	0.986	89.81	1.62×10^5	0.984	82.69	4.02×10^4	0.981	82.91	4.20×10^4	0.980
0.80	127.61	2.86×10^8	0.992	127.07	2.57×10^8	0.992	116.13	3.09×10^8	0.984	90.65	1.91×10^5	0.983	83.42	4.65×10^4	0.980	86.49	8.49×10^4	0.968
Average	**125.38**	**2.13 × 10^8**		**125.42**	**2.09 × 10^8**		**122.35**	**1.30 × 10^8**		**84.81**	**8.64 × 10^4**		**78.30**	**2.27 × 10^4**		**79.41**	**2.69 × 10^4**	
SD*	3.15	1.05×10^8		2.83	9.41×10^7		3.97	8.31×10^7		5.37	5.80×10^4		4.86	1.39×10^4		3.93	2.04×10^4	

* Standard deviation.

between 2.27 × 10^4 s^{-1} and 8.64 × 10^4 s^{-1}. Variation in the pre-exponential factor followed the same trend shown by E_α due to the correlation of these variables (Eq. (21)). Pre-exponential factor values found in this work are in agreement with the results reported in the literature. Slopiecka et al. (2012) noted a pre-exponential factor for poplar wood of 3.80 × 10^6 s^{-1} and 3.93 × 10^6 s^{-1} with an E_α value of 121.97 and 124.40 kJ/mol, respectively. For hazelnut husk, Ceylan and Topçu (2014) found a pre-exponential factor between 2.52 × 10^4 s^{-1} and 1.42 × 10^8 s^{-1} (FWO method), for an E_α of 102.51 kJ/mol and 136.77 kJ/mol, respectively; for KAS method, the pre-exponential factor was 7.5 × 10^3 s^{-1} for an E_α value of 95.01 kJ/mol, and 6.6 × 10^7 s^{-1} for an E_α value of 132.55 kJ/mol.

Thus, E_α resulted to be lower for WCH as compared to WP; thereby, WCH were more reactive, which led to the BC production rate increase under thermochemical processes. This finding was also confirmed by the higher R_a found for WCH (Table 5). Although biochar yield (Y_{char}, Table 1) for WP was ~12 % higher than that one for WCH, WCH burning velocity under gasification was 4.3 times faster than that one found for WP. The higher burning velocity of WCH favors the increment of WCH-BC production rate. Nonetheless, E_α for both raw materials are relatively low. This means that WP and WCH require a low energy input to initiate the pyrolysis reaction (BC production). Furthermore, the devolatilization kinetic data also provide useful information to design and develop new gasification and/or pyrolysis reactors that use patula pine pellets or chips as a feedstock; in addition, data for the thermochemical processes optimization where BC is one of the target products were provided (Lv et al., 2010; Mishra and Mohanty, 2018).

4. Conclusions

The results found in this work indicated that WP (559.97 kg/m^3) showed better properties, as compared to WCH (151.29 kg/m^3), to be used as a feedstock in the co-production of producer gas and BC.

It was found that WP exhibited a better gasification behavior reaching a high CGE (51.59 % and 36.67 % for WP and WCH, respectively), which was ascribed to the higher bulk density and $\dot{V}_{pg}$, and to the lower $\dot{m}_{bms}$ obtained for WP.

The highest gasification temperature reached for WP (391.07 °C) produced a BC with a BET surface area higher than that one for WCH (367.33 m^2/g and 233.56 m^2/g, respectively), because the pores opening and widening. WP-BC HHV was 29.25 MJ/kg, while that one for WCH-BC was 28.36 MJ/kg. This difference was due to the higher content of FC, C and lignin in WP-BC. Both BCs had an aromatic structure, low AC (< 3.0 wt%) and an AI < 0.05 kg-alkali/GJ, resulting in a low corrosion probability. Thus, both BCs could be considered as suitable biofuels.

BCs were observed to be less reactive than the raw biomasses, favoring a higher thermal stability (low fuel consumption) in thermochemical processes. Concerning the raw biomasses, WCH were established to be more reactive with an average E_α of 80.84 kJ/mol (*A*, 2.27 × 10^4 s^{-1} - 8.64 × 10^4 s^{-1}), with regard to WP that reached an average E_α of 124.38 kJ/mol (*A*, 1.30 × 10^8 s^{-1} - 2.13 × 10^8 s^{-1}). This behavior was ascribed to the lower bulk density of WCH, which increased the WCH-BC production rate under pyrolysis regimes.

Author contributions

Jonatan Gutiérrez (First author): data acquisition and curation; investigation; writing the initial draft, and corrections on the manuscript.

Ainhoa Rubio-Clemente (co-author): review and editing, and funding acquisition.

Juan F. Pérez (corresponding author): Conceptualization, writing-review and editing, funding acquisition, and supervision.

Declaration of Competing Interest

The authors report no declarations of interest.

Acknowledgements

The authors acknowledge the financial support of Tecnológico de Antioquia-Institución Universitaria (Colombia) and Universidad de Antioquia through the research project "Valorization of biochars obtained through the microgasification of biomass for water treatment (in Spanish) - FO-INV-07".

Appendix A. Complementary figures for the calculation model of devolatilization kinetic parameters

Fig. A1 shows the conversion variation (α) for the raw biomasses (WP and WCH) as a function of the temperature and heating rates (10, 20, 30, and 40 °C/min). The α calculation was conducted by Eq. (14). In this work, the values of activation energy and pre-exponential coefficient were determined by considering the range $0.2 \leq \alpha_i \leq 0.8$, which corresponded to the range in which the highest devolatilization of biomasses occurred.

Fig. A2 shows isoconversional lines or regression lines in the α_i range, which are required to calculate the activation energy (E_α, kJ/mol) through the Flynn-Wall-Ozawa (FWO), Kissinger-Akahira-Sunose (KAS), and Friedman methods. The referred methods are based on Eqs. (18)–(20), respectively.

The pre-exponential coefficient calculation (A_α, 1/s) was carried out through Eq. (21). For this purpose, T_m (K) determination was required, which is identified as the temperature at which the highest point of the derivative (graph dα/dT *vs* T) was reached , as shown in Fig. A3.

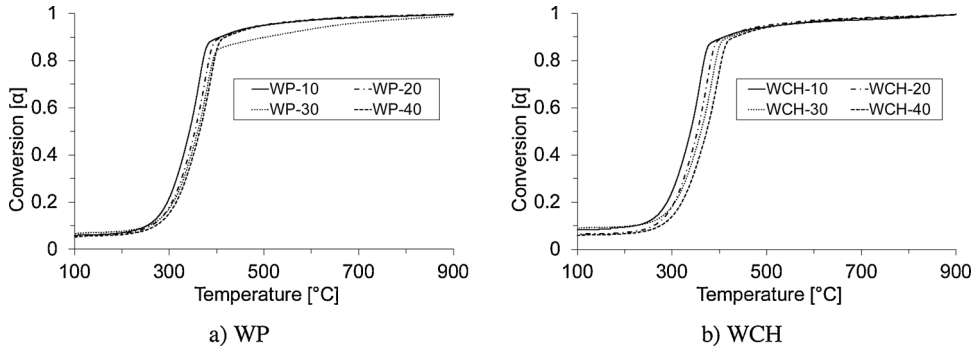

Fig. A1. Conversion grade (α) of WP and WCH used for the devolatilization process at different heating rates.

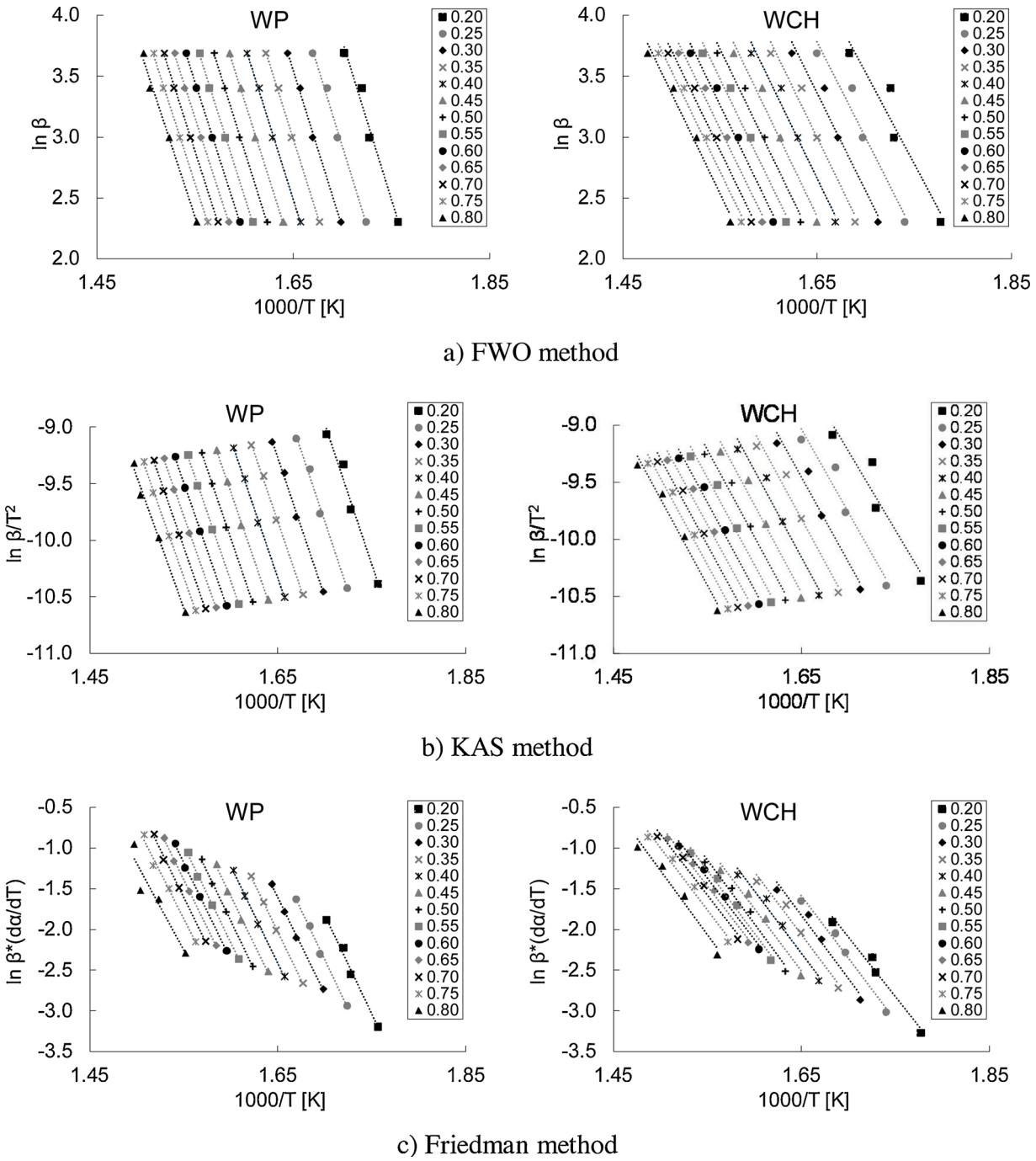

Fig. A2. Regression lines at different values of α used for the activation energy (E_α) calculation.

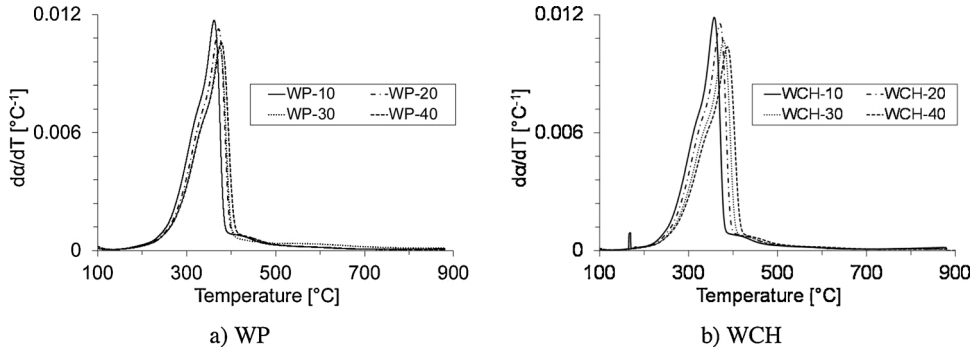

Fig. A3. dα/dT curves at different heating rates used for the pre-exponential coefficient (A_α) calculation.

References

Aboyade, A.O., Hugo, T.J., Carrier, M., Meyer, E.L., Stahl, R., Knoetze, J.H., Görgens, J. F., 2011. Non-isothermal kinetic analysis of the devolatilization of corn cobs and sugar cane bagasse in an inert atmosphere. Thermochim. Acta 517, 81–89. https://doi.org/10.1016/j.tca.2011.01.035.

Antal, M.J., Grønli, M., 2003. The art, science, and technology of charcoal production. Ind. Eng. Chem. Res. 42, 1619–1640. https://doi.org/10.1021/ie0207919.

Arena, U., 2012. Process and technological aspects of municipal solid waste gasification. A review. Waste Manage. 32, 625–639. https://doi.org/10.1016/j.wasman.2011.09.025.

Arteaga-Pérez, L.E., Segura, C., Bustamante-García, V., Cápiro, O.G., Jiménez, R., 2015. Torrefaction of wood and bark from Eucalyptus globulus and Eucalyptus nitens: focus on volatile evolution vs feasible temperatures. Energy 93, 1731–1741. https://doi.org/10.1016/j.energy.2015.10.007.

ASTM, 1996. . Standard Test Method for Gross Calorific Value of Coal and Coke by the Adiabatic Momb Calorimeter. ASTM International, West Conshohocken, PA.

ASTM, 2008. D5373-08 Standard Test Methods for Instrumental Determination of Carbon, Hydrogen, and Nitrogen in Laboratory Samples of Coal. ASTM International, West Conshohocken, PA.

Balat, M., 2007. Influence of coal as an energy source on environmental pollution. Energy Sources, Part A Recover. Util. Environ. Eff. 29, 581–589. https://doi.org/10.1080/15567030701225260.

Bazargan, A., Kostić, M.D., Stamenković, O.S., Veljković, V.B., McKay, G., 2015. A calcium oxide-based catalyst derived from palm kernel shell gasification residues for biodiesel production. Fuel 150, 519–525. https://doi.org/10.1016/j.fuel.2015.02.046.

Biagini, E., Fantei, A., Tognotti, L., 2008. Effect of the heating rate on the devolatilization of biomass residues. Thermochim. Acta 472, 55–63. https://doi.org/10.1016/j.tca.2008.03.015.

Bonilla, J., Salazar, R.P., Mayorga, M., 2019. Kinetic triplet of Colombian sawmill wastes using thermogravimetric analysis. Heliyon 5, e02723. https://doi.org/10.1016/j.heliyon.2019.e02723.

Brewer, C.E., Unger, R., Schmidt-Rohr, K., Brown, R.C., 2011. Criteria to select biochars for field studies based on biochar chemical properties. Bioenergy Res. 4, 312–323. https://doi.org/10.1007/s12155-011-9133-7.

Bridgeman, T.G., Darvell, L.I., Jones, J.M., Williams, P.T., Fahmi, R., Bridgwater, A.V., Barraclough, T., Shield, I., Yates, N., Thain, S.C., Donnison, I.S., 2007. Influence of particle size on the analytical and chemical properties of two energy crops. Fuel 86, 60–72. https://doi.org/10.1016/j.fuel.2006.06.022.

Brudey, T., Largitte, L., Jean-Marius, C., Tant, T., Dumesnil, P.C., Lodewyckx, P., 2016. Adsorption of lead by chemically activated carbons from three lignocellulosic precursors. J. Anal. Appl. Pyrolysis 120, 450–463. https://doi.org/10.1016/j.jaap.2016.06.018.

Castaldi, M., van Deventer, J., Lavoie, J.M., Legrand, J., Nzihou, A., Pontikes, Y., Py, X., Vandecasteele, C., Vasudevan, P.T., Verstraete, W., 2017. Progress and prospects in the field of biomass and waste to energy and added-value materials. Waste Biomass Valorization 8, 1875–1884. https://doi.org/10.1007/s12649-017-0049-0.

Ceylan, S., Topçu, Y., 2014. Pyrolysis kinetics of hazelnut husk using thermogravimetric analysis. Bioresour. Technol. 156, 182–188. https://doi.org/10.1016/j.biortech.2014.01.040.

Chen, B., Chen, Z., 2009. Sorption of naphthalene and 1-naphthol by biochars of orange peels with different pyrolytic temperatures. Chemosphere 76, 127–133. https://doi.org/10.1016/j.chemosphere.2009.02.004.

Chen, W.H., Kuo, P.C., 2010. A study on torrefaction of various biomass materials and its impact on lignocellulosic structure simulated by a thermogravimetry. Energy 35, 2580–2586. https://doi.org/10.1016/j.energy.2010.02.054.

Clare, A., Shackley, S., Joseph, S., Hammond, J., Pan, G., Bloom, A., 2015. Competing uses for China's straw: the economic and carbon abatement potential of biochar. GCB Bioenergy 7, 1272–1282. https://doi.org/10.1111/gcbb.12220.

Congreso de Colombia, 2014. Ley 1715 de 2014. Por medio de la cual se regula la integración de las energías renovables no convencionales al Sistema Energético Nacional.

Daniel, J., Murillo, R., García, T., Arauzo, I., 2014. Thermodynamic analysis for syngas production from volatiles released in waste tire pyrolysis. Energy Convers. Manage. 81, 338–353. https://doi.org/10.1016/j.enconman.2014.02.031.

De Gisi, S., Lofrano, G., Grassi, M., Notarnicola, M., 2016. Characteristics and adsorption capacities of low-cost sorbents for wastewater treatment: a review. Sustain. Mater. Technol. 9, 10–40. https://doi.org/10.1016/j.susmat.2016.06.002.

Díez, H.E., Pérez, J.F., 2017. Physicochemical characterization of representative firewood species used for cooking in some Colombian regions. Int. J. Chem. Eng. 2017, 1–13. https://doi.org/10.1155/2017/4531686.

Díez, H.E., Pérez, J.F., 2019. Effects of wood biomass type and airflow rate on fuel and soil amendment properties of biochar produced in a top-lit updraft gasifier. Environ. Prog. Sustain. Energy 38, 1–14. https://doi.org/10.1002/ep.13105.

Díez, H.E., Gómez, I.N., Pérez, J.F., 2018. Mass, energy, and exergy analysis of the microgasification process in a top-lit updraft reactor: effects of firewood type and forced primary airflow. Sustain. Energy Technol. Assess. 29, 82–91. https://doi.org/10.1016/j.seta.2018.07.003.

Duman, G., Uddin, M.A., Yanik, J., 2014. The effect of char properties on gasification reactivity. Fuel Process. Technol. 118, 75–81. https://doi.org/10.1016/j.fuproc.2013.08.006.

Dunnigan, L., Morton, B.J., Ashman, P.J., Zhang, X., Kwong, C.W., 2018. Emission characteristics of a pyrolysis-combustion system for the co-production of biochar and bioenergy from agricultural wastes. Waste Manage. 77, 59–66. https://doi.org/10.1016/j.wasman.2018.05.004.

Erlich, C., Fransson, T.H., 2011. Downdraft gasification of pellets made of wood, palm-oil residues respective bagasse: experimental study. Appl. Energy 88, 899–908. https://doi.org/10.1016/j.apenergy.2010.08.028.

Estrada, C.A., Melgar, A., Pérez, J.F., 2019. Performance prediction of a decentralized power plant (120 kWe) using a multi-particle model of a downdraft biomass gasification process. Energy Convers. Manage. 181, 258–271. https://doi.org/10.1016/j.enconman.2018.12.002.

Fang, Q., Chen, B., Lin, Y., Guan, Y., 2014. Aromatic and hydrophobic surfaces of wood-derived biochar enhance perchlorate adsorption via hydrogen bonding to oxygen-containing organic groups. Environ. Sci. Technol. 48, 279–288. https://doi.org/10.1021/es403711y.

FAO, 2019. FAOSTAT - Forestry Production and Trade [WWW Document]. http://www.fao.org/faostat/en/#data/FO/visualize.

Gai, C., Dong, Y., Zhang, T., 2013. The kinetic analysis of the pyrolysis of agricultural residue under non-isothermal conditions. Bioresour. Technol. 127, 298–305. https://doi.org/10.1016/j.biortech.2012.09.089.

Gao, X., Wu, H., 2011. Biochar as a fuel: 4. Emission behavior and characteristics of PM 1 and PM 10 from the combustion of pulverized biochar in a drop-tube furnace. Energy Fuels 25, 2702–2710. https://doi.org/10.1021/ef200296u.

García, R., Pizarro, C., Álvarez, A., Lavín, A.G., Bueno, J.L., 2015. Study of biomass combustion wastes. Fuel 148, 152–159. https://doi.org/10.1016/j.fuel.2015.01.079.

Gómez-Barea, A., Ollero, P., Leckner, B., 2013. Optimization of char and tar conversion in fluidized bed biomass gasifiers. Fuel 103, 42–52. https://doi.org/10.1016/j.fuel.2011.04.042.

González, W.A., Pérez, J.F., 2019. CFD analysis and characterization of biochar produced via fixed-bed gasification of fallen leaf pellets. Energy 186. https://doi.org/10.1016/j.energy.2019.115904.

González, W.A., Pérez, J.F., Chapela, S., Porteiro, J., 2018. Numerical analysis of wood biomass packing factor in a fixed-bed gasification process. Renew. Energy 121, 579–589. https://doi.org/10.1016/j.renene.2018.01.057.

González, W.A., López, D., Pérez, J.F., 2020. Biofuel quality analysis of fallen leaf pellets: effect of moisture and glycerol contents as binders. Renew. Energy 147, 1139–1150. https://doi.org/10.1016/j.renene.2019.09.094.

Guerrero, M., Ruiz, M.P., Alzueta, M.U., Bilbao, R., Millera, A., 2005. Pyrolysis of eucalyptus at different heating rates: studies of char characterization and oxidative reactivity. J. Anal. Appl. Pyrolysis 74, 307–314. https://doi.org/10.1016/j.jaap.2004.12.008.

Guo, F., Dong, Y., Dong, L., Guo, C., 2014. Effect of design and operating parameters on the gasification process of biomass in a downdraft fixed bed: an experimental study. Int. J. Hydrogen Energy 39, 5625–5633. https://doi.org/10.1016/j.ijhydene.2014.01.130.

Gupta, R.K., Dubey, M., Kharel, P., Gu, Z., Fan, Q.H., 2015. Biochar activated by oxygen plasma for supercapacitors. J. Power Sources 274, 1300–1305. https://doi.org/10.1016/j.jpowsour.2014.10.169.

Hansen, V., Müller-Stöver, D., Ahrenfeldt, J., Holm, J.K., Henriksen, U.B., Hauggaard-Nielsen, H., 2015. Gasification biochar as a valuable by-product for carbon sequestration and soil amendment. Biomass Bioenergy 72, 300–308. https://doi.org/10.1016/j.biombioe.2014.10.013.

Harvey, L.D.D., 2010. Carbon-Free Energy Supply. Earthscan.

Hernández, J.J., Lapuerta, M., Monedero, E., 2016. Characterisation of residual char from biomass gasification: effect of the gasifier operating conditions. J. Clean. Prod. 138, 83–93. https://doi.org/10.1016/j.jclepro.2016.05.120.

Heydari, M., Rahman, M., Gupta, R., 2015. Kinetic study and thermal decomposition behavior of lignite coal. Int. J. Chem. Eng. 2015, 1–9. https://doi.org/10.1155/2015/481739.

Hubbard, W.G., 2015. Wood bioenergy. Bioenergy 55–71. https://doi.org/10.1016/b978-0-12-407909-0.00004-3.

Iiyama, M., de Nowina, K.R., Mendum, R., Jamnadass, R., Njenga, M., Mahmoud, Y., Sundberg, C., 2017. Quality of charcoal produced using micro gasification and how the new cook stove works in rural Kenya. Environ. Res. Lett. 12, 1–11. https://doi.org/10.1088/1748-9326/aa7499.

Ilyushechkin, A.Y., Roberts, D.G., Harris, D.J., 2014. Characteristics of solid by-products from entrained flow gasification of Australian coals. Fuel Process. Technol. 118, 98–109. https://doi.org/10.1016/j.fuproc.2013.08.017.

International Biochar Initiative [WWW Document], 2019. What Is Biochar? https://biochar-international.org/biochar-in-developing-countries/.

James, R.A.M., Yuan, W., Boyette, M.D., 2016. The effect of biomass physical properties on top-lit updraft gasification of woodchips. Energies 9, 1–13. https://doi.org/10.3390/en9040283.

Jenkins, B.M., Baxter, L.L., Miles, T.R., Miles, T.R., 1998. Combustion properties of biomass. Fuel Process. Technol. 54, 17–46. https://doi.org/10.1016/S0378-3820(97)00059-3.

Jindo, K., Mizumoto, H., Sawada, Y., Sanchez-Monedero, M.A., Sonoki, T., 2014. Physical and chemical characterization of biochars derived from different agricultural residues. Biogeosciences 11, 6613–6621. https://doi.org/10.5194/bg-11-6613-2014.

Kple, M., Girods, P., Anjorin, M., Fagla, B., Rogaume, Y., 2016. Thermal degradation of household solid waste in the town of Abomey-Calavi in Benin: kinetic study. Waste Biomass Valorization 7, 59–70. https://doi.org/10.1007/s12649-015-9441-9.

Laird, D.A., Brown, R.C., Amonette, J.E., Lehmann, J., 2009. Review of the pyrolysis platform for co producing bio-oil and biochar. Biofuels, Bioprod. Biorefining 3, 547–562. https://doi.org/10.1002/bbb.

Lapuerta, M., Hernández, J.J., Pazo, A., López, J., 2008. Gasification and co-gasification of biomass wastes: effect of the biomass origin and the gasifier operating conditions. Fuel Process. Technol. 89, 828–837. https://doi.org/10.1016/j.fuproc.2008.02.001.

Lee, J., Kim, Y., Lee, S., Lee, H., 2012. Optimizing the torrefaction of mixed softwood by response surface methodology for biomass upgrading to high energy density. Bioresour. Technol. 116, 471–476.

Lee, X.J., Lee, L.Y., Gan, S., Thangalazhy-Gopakumar, S., Ng, H.K., 2017. Biochar potential evaluation of palm oil wastes through slow pyrolysis: thermochemical characterization and pyrolytic kinetic studies. Bioresour. Technol. 236, 155–163. https://doi.org/10.1016/j.biortech.2017.03.105.

Lee, M., Lin, Y.L., Chiueh, P.Te, Den, W., 2020. Environmental and energy assessment of biomass residues to biochar as fuel: a brief review with recommendations for future bioenergy systems. J. Clean. Prod. 251, 1–12. https://doi.org/10.1016/j.jclepro.2019.119714.

Lehmann, J., Joseph, S., 2009. Biochar for Environmental Management: Science and Technology. Earthscan, London, UK.

Lenis, Y.A., Pérez, J.F., 2014. Gasification of sawdust and wood chips in a fixed bed under autothermal and stable conditions. Energy Sources, Part A Recover. Util. Environ. Eff. 36, 2555–2565. https://doi.org/10.1080/15567036.2013.875081.

Lenis, Y.A., Pérez, J.F., Melgar, A., 2016. Fixed bed gasification of Jacaranda copaia wood: effect of packing factor and oxygen enriched air. Ind. Crops Prod. 84, 166–175. https://doi.org/10.1016/j.indcrop.2016.01.053.

Lin, X.W., Xie, Z.B., Zheng, J.Y., Liu, Q., Bei, Q.C., Zhu, J.G., 2015. Effects of biochar application on greenhouse gas emissions, carbon sequestration and crop growth in coastal saline soil. Eur. J. Soil Sci. 66, 329–338. https://doi.org/10.1111/ejss.12225.

Liu, Q., Zhong, Z., Wang, S., Luo, Z., 2011. Interactions of biomass components during pyrolysis: a TG-FTIR study. J. Anal. Appl. Pyrolysis 90, 213–218. https://doi.org/10.1016/j.jaap.2010.12.009.

Liu, X., Zhang, Yang, Li, Z., Feng, R., Zhang, Yaozhong, 2014. Characterization of corncob-derived biochar and pyrolysis kinetics in comparison with corn stalk and sawdust. Bioresour. Technol. 170, 76–82. https://doi.org/10.1016/j.biortech.2014.07.077.

Lv, D., Xu, M., Liu, X., Zhan, Z., Li, Z., Yao, H., 2010. Effect of cellulose, lignin, alkali and alkaline earth metallic species on biomass pyrolysis and gasification. Fuel Process. Technol. 91, 903–909. https://doi.org/10.1016/j.fuproc.2009.09.014.

Lv, J., Ao, X., Li, Q., Cao, Y., Chen, Q., Xie, Y., 2019. Steam co-gasification of different ratios of spirit-based distillers' grains and anthracite coal to produce hydrogen-rich gas. Bioresour. Technol. 283, 59–66. https://doi.org/10.1016/j.biortech.2019.03.047.

Maiti, S., Dey, S., Purakayastha, S., Ghosh, B., 2006. Physical and thermochemical characterization of rice husk char as a potential biomass energy source. Bioresour. Technol. 97, 2065–2070. https://doi.org/10.1016/j.biortech.2005.10.005.

Martínez-Ángel, J.D., Villamizar-Gallardo, R.A., Ortíz-Rodríguez, O.O., 2015. Characterization and evaluation of cocoa (Theobroma cacao L.) pod husk as a renewable energy source. Agrociencia 49, 329–345.

Medic, D., Darr, M., Shah, A., Potter, B., Zimmerman, J., 2012. Effects of torrefaction process parameters on biomass feedstock upgrading. Fuel 91, 147–154. https://doi.org/10.1016/j.fuel.2011.07.019.

Minagricultura, 2015. Colombia tiene un potencial forestal de 24 millones de hectáreas para explotación comercial [WWW Document] (accessed 4.14.20). https://www.minagricultura.gov.co/noticias/Paginas/Colombia-tiene-un-potencial-forestal.aspx.

Misginna, M.T., Rajabu, H.M., 2014. The potential of charcoal making stove to enhance energy efficiency. Int. J. Innov. Appl. Stud. 5, 206–214.

Mishra, R.K., Mohanty, K., 2018. Pyrolysis kinetics and thermal behavior of waste sawdust biomass using thermogravimetric analysis. Bioresour. Technol. 251, 63–74. https://doi.org/10.1016/j.biortech.2017.12.029.

Montgomery, D.C., 2004. Design and Analysis of Experiments, second edi. Limusa Wiley. LIMUSA, S.A, Arizona. https://doi.org/10.1080/00224065.2014.11917962.

Montiel-Bohórquez, N.D., Pérez, J.F., 2019. Generación de energía a partir de residuos sólidos urbanos. estrategias termodinámicas para optimizar el desempeño de centrales térmicas. Inf. tecnológica 30, 273–284. https://doi.org/10.4067/s0718-07642019000100273.

Montoya, J., Pecha, B., Roman, D., Janna, F.C., Garcia-Perez, M., 2017. Effect of temperature and heating rate on product distribution from the pyrolysis of sugarcane bagasse in a hot plate reactor. J. Anal. Appl. Pyrolysis 123, 347–363. https://doi.org/10.1016/j.jaap.2016.11.008.

Nanda, S., Mohanty, P., Pant, K.K., Naik, S., Kozinski, J.A., Dalai, A.K., 2013. Characterization of North American lignocellulosic biomass and biochars in terms of their Candidacy for alternate renewable fuels. Bioenergy Res. 6, 663–677. https://doi.org/10.1007/s12155-012-9281-4.

Novaes, E., Kirst, M., Chiang, V., Winter-sederoff, H., Sederoff, R., 2010. Lignin and biomass : a negative correlation for wood formation and lignin content in trees. Am. Soc. Plant Biol. 154, 555–561. https://doi.org/10.1104/pp.110.161281.

Nyakuma, B.B., Ahmad, A., Johari, A., Abdullah, T.A.T., Oladokun, O., Aminu, D.Y., 2015. Non-isothermal kinetic analysis of oil palm empty fruit bunch pellets by thermogravimetric analysis. Chem. Eng. Trans. 45, 1327–1332. https://doi.org/10.3303/CET1545222.

Nzioka, A.M., Kim, M.G., Hwang, H.U., Kim, Y.J., 2019. Kinetic study of the thermal decomposition process of municipal solid waste using TGA. Waste Biomass Valorization 10, 1679–1691. https://doi.org/10.1007/s12649-017-0183-8.

Ok, Y., Uchimiya, S., Chang, S., Bolan, N., 2016. Biochar: Production, Characterization, and Applications. CRC Press, Taylor & Francis Group, New York.

Osorio, L.F., Del Valle, J., Restrepo, H., 2014. Valoración del potencial energético de núcleos forestales, en Biomasa forestal como alternativa energética. Análisis silvicultural, técnico y financiero de poryectos, 1ra ed. Editorial Universidad de Antioquia, Medellín (Colombia).

Pérez, J.F., Ramírez, G.L., 2019. Aplicaciones agroenergéticas con maderas cultivadas y oportunidades preliminares de mercado, 1st ed. Editorial Universidad de Antioquia. Editorial Universidad de Antioquia, Medellín (Colombia).

Pérez, J.F., Melgar, A., Benjumea, P.N., 2012. Effect of operating and design parameters on the gasification/combustion process of waste biomass in fixed bed downdraft reactors: an experimental study. Fuel 96, 487–496. https://doi.org/10.1016/j.fuel.2012.01.064.

Perez, J.F., Benjumea, P.N., Melgar, A., 2015. Sensitivity analysis of a biomass gasification model in fixed bed downdraft reactors: effect of model and process parameters on reaction front. Biomass Bioenergy 83, 403–421. https://doi.org/10.1016/j.biombioe.2015.10.014.

Pérez, J.F., Osorio, L.F., Agudelo, A.F., 2018. A technical-economic analysis of wood gasification for decentralized power generation in colombian forest cores. Int. J. Renew. Energy Res. 8, 1071–1084.

Pérez, J.F., Pelaez-Samaniego, M.R., Garcia-Perez, M., 2019. Torrefaction of fast-growing Colombian wood species. Waste Biomass Valorization 10, 1655–1667. https://doi.org/10.1007/s12649-017-0164-y.

Porteiro, J., Patiño, D., Collazo, J., Granada, E., Moran, J., Miguez, J.L., 2010. Experimental analysis of the ignition front propagation of several biomass fuels in a fixed-bed combustor. Fuel 89, 26–35. https://doi.org/10.1016/j.fuel.2009.01.024.

Protásio, T., de, P., Bufalino, L., Denzin, G.H., Junior, M.G., Trugilho, P.F., Mendes, L.M., 2013. Brazilian lignocellulosic wastes for bioenergy production: characterization and comparison with fossil fuels. BioResources 8, 1166–1185. https://doi.org/10.15376/biores.8.1.1166-1185.

Qian, K., Kumar, A., Patil, K., Bellmer, D., Wang, D., Yuan, W., Huhnke, R.L., 2013. Effects of biomass feedstocks and gasification conditions on the physiochemical properties of char. Energies 6, 3972–3986. https://doi.org/10.3390/en6083972.

Qian, L., Zhao, Y., Sun, S., Che, H., Chen, H., Wang, D., 2014. Chemical/physical properties of char during devolatilization in inert and reducing conditions. Fuel Process. Technol. 118, 327–334. https://doi.org/10.1016/j.fuproc.2013.09.012.

Qian, K., Kumar, A., Zhang, H., Bellmer, D., Huhnke, R., 2015. Recent advances in utilization of biochar. Renew. Sustain. Energy Rev. 42, 1055–1064. https://doi.org/10.1016/j.rser.2014.10.074.

Ramos-Carmona, S., Delgado-Balcázar, S., Pérez, J.F., 2017. Physicochemical characterization of torrefied wood biomass under air as oxidizing atmosphere. BioResources 12, 5428–5448. https://doi.org/10.15376/biores.12.3.5428-5448.

Ramos-Carmona, S., Martínez, J.D., Pérez, J.F., 2018. Torrefaction of patula pine under air conditions: a chemical and structural characterization. Ind. Crops Prod. 118, 302–310. https://doi.org/10.1016/j.indcrop.2018.03.062.

Ren, J., Liu, Y.L., Zhao, X.Y., Cao, J.P., 2019. Biomass thermochemical conversion: a review on tar elimination from biomass catalytic gasification. J. Energy Inst. 93, 1083–1098. https://doi.org/10.1016/j.joei.2019.10.003.

Saghir, M., Rehan, M., Nizami, A.-S., 2018. Recent trends in gasification based waste-to-energy. Gasif. Low-grade Feed., pp. 97–114. https://doi.org/10.5772/intechopen.74487.

Santos, N.A.V., Magriotis, Z.M., Saczk, A.A., Fássio, G.T.A., Vieira, S.S., 2015. Kinetic study of pyrolysis of castor beans (Ricinus communis L.) presscake: an alternative use for solid waste arising from the biodiesel production. Energy Fuels 29, 2351–2357. https://doi.org/10.1021/ef401933c.

Shin, D., Choi, S., 2000. The combustion of simulated waste particles in a fixed bed. Combust. Flame 121, 167–180. https://doi.org/10.1016/S0010-2180(99)00124-8.

Sikarwar, V.S., Zhao, M., Clough, P., Yao, J., Zhong, X., Memon, M.Z., Shah, N., Anthony, E.J., Fennell, P.S., 2016. An overview of advances in biomass gasification. Energy Environ. Sci. 9, 2939–2977. https://doi.org/10.1039/c6ee00935b.

Slopiecka, K., Bartocci, P., Fantozzi, F., 2012. Thermogravimetric analysis and kinetic study of poplar wood pyrolysis. Appl. Energy 97, 491–497. https://doi.org/10.1016/j.apenergy.2011.12.056.

Sobek, S., Werle, S., 2020. Kinetic modelling of waste wood devolatilization during pyrolysis based on thermogravimetric data and solar pyrolysis reactor performance. Fuel 261. https://doi.org/10.1016/j.fuel.2019.116459.

Sohi, S.P., Krull, E., Lopez-Capel, E., Bol, R., 2010. A review of biochar and its use and function in soil. Adv. Agron. 105, 47–82. https://doi.org/10.1016/S0065-2113(10)05002-9.

Teixeira, P., Lopes, H., Gulyurtlu, I., Lapa, N., Abelha, P., 2012. Evaluation of slagging and fouling tendency during biomass co-firing with coal in a fluidized bed. Biomass Bioenergy 39, 192–203. https://doi.org/10.1016/j.biombioe.2012.01.010.

Tinaut, F.V., Melgar, A., Pérez, J.F., Horrillo, A., 2008. Effect of biomass particle size and air superficial velocity on the gasification process in a downdraft fixed bed gasifier. An experimental and modelling study. Fuel Process. Technol. 89, 1076–1089. https://doi.org/10.1016/j.fuproc.2008.04.010.

Vamvuka, D., Pitharoulis, M., Alevizos, G., Repouskou, E., Pentari, D., 2009. Ash effects during combustion of lignite/biomass blends in fluidized bed. Renew. Energy 34, 2662–2671. https://doi.org/10.1016/j.renene.2009.05.005.

van Soest, P.J., Robertson, J.B., Lewis, Ba., 1991v. Methods for dietary fiber, neutral detergent fiber, and nonstarch polysaccharides in relation to animal nutrition. J. Dairy Sci. 74, 3583–3597. https://doi.org/10.3168/jds.S0022-0302(91)78551-2.

Vyazovkin, S., Burnham, A.K., Criado, J.M., Pérez-Maqueda, L.A., Popescu, C., Sbirrazzuoli, N., 2011. ICTAC Kinetics Committee recommendations for performing kinetic computations on thermal analysis data. Thermochim. Acta 520, 1–19. https://doi.org/10.1016/j.tca.2011.03.034.

Wang, Y., Yin, R., Liu, R., 2014. Characterization of biochar from fast pyrolysis and its effect on chemical properties of the tea garden soil. J. Anal. Appl. Pyrolysis 110, 375–381. https://doi.org/10.1016/j.jaap.2014.10.006.

Whittaker, C., Shield, I., 2016. Short rotation woody energy crop supply chains. Biomass Supply Chain. Bioenergy Biorefining, pp. 217–248. https://doi.org/10.1016/B978-1-78242-366-9.00010-1.

Xie, H., Yu, Q., Qin, Q., Zhang, H., Li, P., 2013. Study on pyrolysis characteristics and kinetics of biomass and its components. J. Renew. Sustain. Energy 5, 1–15. https://doi.org/10.1063/1.4792845.

Zapata, R.B., Bayer, J.F.P., Jiménez, C.S., 2014. Colombian coals : classification and thermochemical characterization for energy applications. Rev. Ion 27, 43–54.

Zha, Q., Bu, Y., Wang, C., Che, D., 2016. Evaluation of anthracite combustion and NOx emissions under oxygen-staging, high-temperature conditions. Appl. Therm. Eng. 109, 751–760. https://doi.org/10.1016/j.applthermaleng.2016.08.109.

Zhang, Y., Ashizawa, M., Kajitani, S., Miura, K., 2008. Proposal of a semi-empirical kinetic model to reconcile with gasification reactivity profiles of biomass chars. Fuel 87, 475–481. https://doi.org/10.1016/j.fuel.2007.04.026.